# SELF-CONTAINED FILTERED DENSITY FUNCTION

by

**Arash G. Nouri**

B.S. and M.S. in Mechanical Engineering, Sharif University of Technology, Tehran, 2010, 2013

M.S. in Chemical Engineering, University of Pittsburgh, Pittsburgh, 2016

Submitted to the Graduate Faculty of
the Swanson School of Engineering in partial fulfillment
of the requirements for the degree of

**Doctor of Philosophy**

University of Pittsburgh

2017

UNIVERSITY OF PITTSBURGH

SWANSON SCHOOL OF ENGINEERING

This dissertation was presented

by

Arash G. Nouri

It was defended on

September 27, 2017

and approved by

Peyman Givi, Ph.D., Distinguished Professor, and James T. MacLeod Professor, Department of Mechanical Engineering and Materials Science

William J. Layton, Ph.D., Professor, Department of Mathematics

Sangyeop Lee, Ph.D., Assistant Professor, Department of Mechanical Engineering and Materials Science

Satbir Singh, Ph.D., Assistant Professor, Department of Mechanical Engineering, Carnegie Mellon University

Dissertation Director: Peyman Givi, Ph.D., Distinguished Professor, and James T. MacLeod Professor, Department of Mechanical Engineering and Materials Science

**SELF-CONTAINED FILTERED DENSITY FUNCTION**

Arash G. Nouri, PhD

University of Pittsburgh, 2017

The filtered density function (FDF) closure is extended to a "self-contained" format to include the subgrid scale (SGS) statistics of all of the hydro-thermo-chemical variables in turbulent flows. These are the thermodynamic pressure, the specific internal energy, the velocity vector, and the composition field. In this format, the model is comprehensive and facilitates large eddy simulation (LES) of flows at both low and high compressibility levels. A transport equation is developed for the joint "pressure-energy-velocity-composition filtered mass density function (PEVC-FMDF)." In this equation, the effect of convection appears in closed form. The coupling of the hydrodynamics and thermochemistry is modeled via a set of stochastic differential equation (SDE) for each of the transport variables. This yields a self-contained SGS closure. For demonstration, LES is conducted of a turbulent shear flow with transport of a passive scalar. The consistency of the PEVC-FMDF formulation is established, and its overall predictive capability is appraised via comparison with direct numerical simulation (DNS) data.

**Keywords:** Large eddy simulation; filtered density function; Monte Carlo methods; compressible turbulent flows.

## TABLE OF CONTENTS

## LIST OF FIGURES

## PREFACE

I would like to express my sincere appreciation to my advisor, Professor Peyman Givi for his support and guidance through the course of my graduate studies. I would like to thank the members of my doctoral committee, Professors William Layton, Sangyeop Lee and Satbir Singh (Carnegie Mellon University). My appreciation also goes to Dr. Mehdi B. Nik (Stanford University) and Dr. Daniel Livescu (Los Alamos National Laboratory) for their friendship and collaboration on many technical aspects of my research. I owe special thanks to Professor Stephen B. Pope (Cornell University) whose insights and collaborations contributed greatly to the success of this work. I would like to acknowledge Professor Cyrus K. Madnia (University at Buffalo) for his collaboration on several technical issues of this dissertation.

I am indebted to my colleagues and friends whom I had the pleasure to work with at one point or another during my time at the University of Pittsburgh: Mr. Cajon Gonzales, Mr. Medet Inkarbekov, Ms. Wendy Janocha, Dr. Patrick Pisciuneri, Dr. Sasan Salkhordeh, Dr. Shervin Sammak and Mr. Krisda Tapracharoen. My deepest gratitude goes to my parents Mohammad and Zhila, and my sisters Farnoush and Shima; for their love and support. I dedicate this thesis to them.

This work is sponsored by AFOSR under Grant No. FA9550-12-1-0057 and by NSF under Grants No. CBET-1603131 and No. CBET-1609120. Computational resources are provided by the University of Pittsburgh Center for Research Computing.

ARASH G. NOURI

UNIVERSITY OF PITTSBURGH, 2017

## 1.0 INTRODUCTION

The filtered density function (FDF) and its density weighted filtered mass density function (FMDF) have proven very effective for large eddy simulation (LES) of turbulent flows.[1–8] The most sophisticated form of the model to-date is one accounting for the joint frequency-velocity-scalar subgrid scale (SGS) statistics (FVS-FMDF),[9] and a simpler version (VS-FMDF) which does not include the SGS frequency.[10–12] Inclusion of entropy and irreversibility is reported in Refs.,[13–15] and extension to multi-phase flows in Refs.[16,17] Hydrodynamic closure in incompressible, non-reacting flows has been achieved via the marginal velocity-FDF (V-FDF),[18] and the FDF which considers only the species mass fraction field is the scalar-FDF (S-FDF and S-FMDF).[19] This is the most elementary form of the model,[20–24] and has experienced widespread applications for LES of a variety of reactive flows. Some examples are in Refs;[25–47] see Ref.[1] for a recent review. In almost all of these contributions, the FDF is considered for flows at low compressibility levels. As such, the effects of pressure fluctuations in the energy transport is negligible, and the latter is governed by a scalar equation similar to that for the composition. Some corrections to account for the effects of pressure in LES of compressible flows have been attempted.[48–50]

## 1.1 OBJECTIVE AND SCOPE

The objective of the present work is to extend the FDF methodology to a "self-contained" manner for flows with both low and high levels of compressibility. This is facilitated by SGS modeling of *all* of the pertinent transport variables of compressible flows, as required for a stand-alone description. The central part of the formulation is the "pressure" term

which provides the coupling between hydrodynamics and thermochemistry. This term is coupled with the internal energy, the fluid velocity, and the composition field. Consistent with established terminology, the resulting model is termed PEVC-FMDF. With the formal definition of PEVC-FMDF, the mathematical framework for its implementation in LES is established. A transport equation is developed for the PEVC-FMDF in which the effect of the SGS convection appears in closed form. The unclosed terms are modeled via a set of stochastic differential equations (SDEs). Since the FDF is a single-point descriptor, all of the multi-point statistics are also modeled externally. A Lagrangian Monte Carlo procedure is developed and implemented for the numerical solution of these SDEs. Simulations are conducted of a turbulent shear flow with variable levels of compressibility. The consistency and the overall capability of the closure is assessed via comparison with direct numerical simulation (DNS) data.

The work described in this dissertation has been presented at *ICMIDS*[51] and *APS-DFD*[52–54] and is published in *Physical Review Fluids*.[55] Some parts of this dissertation were also the subject of (*i*) an invited talk at the *CITech 2015* Conference which was subsequently published in an invited tutorial book chapter,[56] and (*ii*) a chapter in *Combustion for Power Generation and Transportation* monograph.[57]

# 2.0 FORMULATION

## 2.1 BASIC EQUATIONS

For the mathematical description of compressible flows involving $N_s$ species, the primary transport variables are the density $\rho(\mathbf{x},t)$, velocity vector $u_i(\mathbf{x},t)$ $(i=1,2,3)$, pressure $p(\mathbf{x},t)$, temperature $T(\mathbf{x},t)$, internal energy $e(\mathbf{x},t)$, and species mass fractions $\phi_\alpha(\mathbf{x},t)$ $(\alpha = 1..N_s)$. The equations which govern the transport of the above variables in space $(x_i)$ and time $(t)$ are the continuity, conservation of momentum, internal energy, and species mass fractions:

$$\frac{\partial \rho}{\partial t} + \frac{\partial \rho u_j}{\partial x_j} = 0, \tag{2.1a}$$

$$\frac{\partial \rho u_i}{\partial t} + \frac{\partial \rho u_i u_j}{\partial x_j} = -\frac{\partial p}{\partial x_i} + \frac{\partial \tau_{ij}}{\partial x_j}, \tag{2.1b}$$

$$\frac{\partial \rho e}{\partial t} + \frac{\partial \rho e u_j}{\partial x_j} = -\frac{\partial q_j}{\partial x_j} + \sigma_{ij}\frac{\partial u_i}{\partial x_j}, \tag{2.1c}$$

$$\frac{\partial \rho \phi_\alpha}{\partial t} + \frac{\partial \rho \phi_\alpha u_j}{\partial x_j} = -\frac{\partial J_j^\alpha}{\partial x_j}, \quad \alpha = 1,2,...,N_s. \tag{2.1d}$$

For a Newtonian fluid, the viscous stress tensor $\tau_{ij}$, the heat flux $q_j$, the species $\alpha$ diffusive mass flux vector $J_j^\alpha$, and $\sigma_{ij}$ tensor are represented by

$$\tau_{ij} = \mu\left(\frac{\partial u_i}{\partial x_j} + \frac{\partial u_j}{\partial x_i} - \frac{2}{3}\frac{\partial u_k}{\partial x_k}\,\delta_{ij}\right), \tag{2.2a}$$

$$q_j = -\lambda\frac{\partial T}{\partial x_j}, \tag{2.2b}$$

$$J_j^\alpha = -\rho\Gamma_\alpha \frac{\partial \phi_\alpha}{\partial x_j}, \tag{2.2c}$$

$$\sigma_{ij} = \tau_{ij} - p\delta_{ij}, \tag{2.2d}$$

where $\mu$ is the fluid dynamic viscosity, $\lambda$ is the thermal conductivity, and $\Gamma_\alpha$ denotes the mass diffusion coefficient. To put the equations in a compact form, and for compatibility with the simulation results presented in the next section, we assume a perfect gas with the specific heat ratio $\gamma = c_p/c_v$, and internal energy $de = c_v dT$; where $c_p$ and $c_v$ denote the specific heats at constant pressure and constant volume, respectively and are assumed to be constants. The diffusion coefficients are the same for all of the species ($\Gamma_\alpha = \Gamma_\beta = \Gamma$) ; and we assume $\mu = \rho\Gamma$ and $c_v\mu = \lambda$, i.e., unity Schmidt ($Sc = \frac{\mu}{\rho\Gamma}$) and Prandtl ($Pr = \frac{c_v\mu}{\lambda}$) numbers. The viscosity and molecular diffusivity coefficients can, in general, be temperature dependent but in this initial study, they are assumed to be constants. In reactive flows, molecular processes and thermodynamics are much more complicated than portrayed here. These are not our primary concern here, so the simple model is adopted with justifications and caveats given in Refs.[58–60] With these assumptions, the equation of state is expressed as

$$p = \rho R^0 T/\overline{M} = \rho R T = (\gamma - 1)\rho e, \tag{2.3}$$

where $R^0$ and $R$ are the universal and mixture gas constants, and $\overline{M}$ is the molecular weight for the mixture. Therefore, the pressure is governed by[61]

$$\frac{\partial p}{\partial t} + \frac{\partial p u_j}{\partial x_j} = -(\gamma - 1)\frac{\partial q_j}{\partial x_j} + (\gamma - 1)\sigma_{ij}\frac{\partial u_i}{\partial x_j}. \tag{2.4}$$

## 2.2 FILTERED EQUATIONS

Large eddy simulation involves the spatial filtering operation[62–66]

$$\langle Q(\mathbf{x}, t)\rangle_\ell = \int_{-\infty}^{+\infty} Q(\mathbf{x}', t) G_{\Delta_1}(\mathbf{x}', \mathbf{x}) d\mathbf{x}', \tag{2.5}$$

where $G_{\Delta_1}(\mathbf{x}', \mathbf{x})$ denotes a filter function, and $\langle Q(\mathbf{x}, t)\rangle_\ell$ is the filtered value of the transport variable $Q(\mathbf{x}, t)$. In this definition, the subscript "1" for the filter function indicates that $\langle Q(\mathbf{x}, t)\rangle_\ell$ is the first level filter value of variable $Q(\mathbf{x}, t)$.[67] In variable-density flows it is convenient to use the Favre-filtered quantity $\langle Q(\mathbf{x}, t)\rangle_L = \langle \rho Q\rangle_\ell / \langle \rho\rangle_\ell$. We consider a filter function that is spatially and temporally invariant and localized, thus: $G_{\Delta_1}(\mathbf{x}', \mathbf{x}) \equiv G_{\Delta_1}(\mathbf{x}' - \mathbf{x})$ with the properties $G_{\Delta_1}(\mathbf{x}) \geq 0$, and $\int_{-\infty}^{+\infty} G_{\Delta_1}(\mathbf{x}) d\mathbf{x} = 1$. Also, the second level spatial filtering operation is defined as

$$\langle\langle Q(\mathbf{x}, t)\rangle_\ell\rangle_{\ell_2} = \int_{-\infty}^{+\infty} \langle Q(\mathbf{x}', t)\rangle_\ell \, G_{\Delta_2}(\mathbf{x}', \mathbf{x}) d\mathbf{x}', \tag{2.6}$$

where $G_{\Delta_2}(\mathbf{x}', \mathbf{x})$ denotes a secondary filter function. Similar to the first level filtering operation, $\langle\langle Q(\mathbf{x}, t)\rangle_L\rangle_{L_2} = \langle\langle \rho Q\rangle_\ell\rangle_{\ell_2} / \langle\langle \rho\rangle_\ell\rangle_{\ell_2}$. Applying the first level filtering operation to Eqs. (2.1) and (2.4) and using the conventional LES approximation for the diffusion terms, we obtain

$$\frac{\partial \langle \rho\rangle_\ell}{\partial t} + \frac{\partial \langle \rho\rangle_\ell \langle u_j\rangle_L}{\partial x_j} = 0, \tag{2.7a}$$

$$\frac{\partial \langle \rho\rangle_\ell \langle u_i\rangle_L}{\partial t} + \frac{\partial \langle \rho\rangle_\ell \langle u_j\rangle_L \langle u_i\rangle_L}{\partial x_j} = -\frac{\partial \langle p\rangle_\ell}{\partial x_i} + \frac{\partial \breve{\tau}_{ij}}{\partial x_j} - \frac{\partial \langle \rho\rangle_\ell \tau_L(u_i, u_j)}{\partial x_j}, \tag{2.7b}$$

$$\begin{aligned}\frac{\partial \langle \rho\rangle_\ell \langle e\rangle_L}{\partial t} + \frac{\partial \langle \rho\rangle_\ell \langle u_j\rangle_L \langle e\rangle_L}{\partial x_j} = &-\frac{\partial \breve{q}_j}{\partial x_j} - \frac{\partial \langle \rho\rangle_\ell \tau_L(e, u_j)}{\partial x_j} + \breve{\tau}_{ij}\frac{\partial \langle u_i\rangle_L}{\partial x_j} \\ &+ \epsilon - \Pi_d - \langle p\rangle_\ell \frac{\partial \langle u_i\rangle_\ell}{\partial x_i},\end{aligned} \tag{2.7c}$$

$$\frac{\partial \langle \rho\rangle_\ell \langle \phi_\alpha\rangle_L}{\partial t} + \frac{\partial \langle \rho\rangle_\ell \langle u_j\rangle_L \langle \phi_\alpha\rangle_L}{\partial x_j} = -\frac{\partial \breve{J}_j^\alpha}{\partial x_j} - \frac{\partial \langle \rho\rangle_\ell \tau_L(\phi_\alpha, u_j)}{\partial x_j}, \tag{2.7d}$$

$$\frac{\partial \langle p\rangle_\ell}{\partial t}+\frac{\partial \langle p\rangle_\ell \langle u_j\rangle_\ell}{\partial x_j}=-(\gamma-1)\frac{\partial \breve{q}_j}{\partial x_j}-\frac{\partial \tau_\ell(p,u_j)}{\partial x_j}$$

$$+(\gamma-1)\breve{\tau}_{ij}\frac{\partial \langle u_i\rangle_L}{\partial x_j}+(\gamma-1)\epsilon$$

$$-(\gamma-1)\Pi_d-(\gamma-1)\langle p\rangle_\ell \frac{\partial \langle u_i\rangle_\ell}{\partial x_i}. \tag{2.7e}$$

In Eq. (2.7), the filtered viscous stress tensor $\breve{\tau}_{ij}$, the filtered energy flux $\breve{q}_j$ and the filtered diffusive mass flux vector $\breve{J}_j^\alpha$ are defined as

$$\breve{\tau}_{ij} = \mu\left(\frac{\partial \langle u_i\rangle_L}{\partial x_j}+\frac{\partial \langle u_j\rangle_L}{\partial x_i}-\frac{2}{3}\frac{\partial \langle u_k\rangle_L}{\partial x_k}\delta_{ij}\right), \tag{2.8a}$$

$$\breve{q}_j = -\lambda\frac{\partial \langle T\rangle_L}{\partial x_j}, \tag{2.8b}$$

$$\breve{J}_j^\alpha = -\langle\rho\rangle_\ell \Gamma\frac{\partial \langle \phi_\alpha\rangle_L}{\partial x_j}, \tag{2.8c}$$

$$\Pi_d = \left\langle p\frac{\partial u_i}{\partial x_i}\right\rangle_\ell-\langle p\rangle_\ell\frac{\partial \langle u_i\rangle_\ell}{\partial x_i}, \tag{2.8d}$$

$$\epsilon = \left\langle \tau_{ij}\frac{\partial u_i}{\partial x_j}\right\rangle_\ell-\breve{\tau}_{ij}\frac{\partial \langle u_i\rangle_L}{\partial x_j}. \tag{2.8e}$$

The second-order and third-order regular SGS correlations and Favre SGS correlations are defined by

$$\tau_\ell(a,b) = \langle ab\rangle_\ell-\langle a\rangle_\ell\langle b\rangle_\ell, \tag{2.9a}$$

$$\tau_\ell(a,b,c) = \langle abc\rangle_\ell-\langle a\rangle_\ell\tau_\ell(b,c)-\langle b\rangle_\ell\tau_\ell(a,c)-\langle c\rangle_\ell\tau_\ell(a,c)-\langle a\rangle_\ell\langle b\rangle_\ell\langle c\rangle_\ell, \tag{2.9b}$$

$$\tau_L(a,b) = \langle ab\rangle_L-\langle a\rangle_L\langle b\rangle_L, \tag{2.9c}$$

$$\tau_L(a,b,c) = \langle abc\rangle_L-\langle a\rangle_L\tau_L(b,c)-\langle b\rangle_L\tau_L(a,c)-\langle c\rangle_L\tau_L(a,c)-\langle a\rangle_L\langle b\rangle_L\langle c\rangle_L. \tag{2.9d}$$

The second order velocity correlations are governed by

$$\frac{\partial \langle\rho\rangle_\ell \tau_L(u_i,u_j)}{\partial t} + \frac{\partial \langle\rho\rangle_\ell \langle u_k\rangle_L \tau_L(u_i,u_j)}{\partial x_k} = \langle\rho\rangle_\ell P_{ij} - \frac{\partial T_{ijk}}{\partial x_k} - \epsilon_{ij} + \Pi_{ij}. \quad (2.10)$$

Equation (2.10) provides an "exact" form of the transport equations for the second order velocity correlations. In this equation, the production term $P_{ij}$, the transport term $T_{ijk}$, the dissipation term $\epsilon_{ij}$ and the pressure-rate-of-strain tensor $\Pi_{ij}$ are defined as

$$P_{ij} = -\tau_L(u_i,u_k)\frac{\partial \langle u_j\rangle_L}{\partial x_k} - \tau_L(u_j,u_k)\frac{\partial \langle u_i\rangle_L}{\partial x_k}, \quad (2.11a)$$

$$\begin{aligned} T_{ijk} &= \langle\rho\rangle_\ell \tau_L(u_i,u_j,u_k) + \tau(p,u_i)\delta_{jk} + \tau(p,u_j)\delta_{ik} \\ &- (\tau(u_i,\tau_{jk}) + \tau(u_j,\tau_{ik})), \end{aligned} \quad (2.11b)$$

$$\epsilon_{ij} = \left(\left\langle \tau_{ik}\frac{\partial u_j}{\partial x_k}\right\rangle_\ell - \breve{\tau}_{ik}\frac{\partial \langle u_j\rangle_L}{\partial x_k}\right) + \left(\left\langle \tau_{jk}\frac{\partial u_i}{\partial x_k}\right\rangle_\ell - \breve{\tau}_{jk}\frac{\partial \langle u_i\rangle_L}{\partial x_k}\right), \quad (2.11c)$$

$$\Pi_{ij} = \left(\left\langle p\frac{\partial u_i}{\partial x_j}\right\rangle_\ell - \langle p\rangle_\ell \frac{\partial \langle u_i\rangle_L}{\partial x_j}\right) + \left(\left\langle p\frac{\partial u_j}{\partial x_i}\right\rangle_\ell - \langle p\rangle_\ell \frac{\partial \langle u_j\rangle_L}{\partial x_i}\right). \quad (2.11d)$$

In Eq. (2.11b), the subgrid terms without the subscript are defined as

$$\tau(p,u_i) = \langle pu_i\rangle_\ell - \langle p\rangle_\ell \langle u_i\rangle_L, \quad (2.12a)$$

$$\tau(p,u_j) = \langle pu_j\rangle_\ell - \langle p\rangle_\ell \langle u_j\rangle_L, \quad (2.12b)$$

$$\tau(u_i,\tau_{jk}) = \langle u_i\tau_{jk}\rangle_\ell - \langle u_i\rangle_L \breve{\tau}_{jk}, \quad (2.12c)$$

$$\tau(u_j,\tau_{ik}) = \langle u_j\tau_{ik}\rangle_\ell - \langle u_j\rangle_L \breve{\tau}_{ik}. \quad (2.12d)$$

From Eqs. (2.8e) and (2.11c), the dissipation is defined as: $\epsilon = \epsilon_{ii}/2$.

The second order velocity-scalar correlations are governed by

$$\frac{\partial \langle\rho\rangle_\ell \tau_L(u_i,\phi_\alpha)}{\partial t} + \frac{\partial \langle\rho\rangle_\ell \langle u_k\rangle_L \tau_L(u_i,\phi_\alpha)}{\partial x_k} = \langle\rho\rangle_\ell P_i^\alpha - \frac{\partial T_{ik}^\alpha}{\partial x_k} - \epsilon_i^\alpha + \Pi_i^\alpha. \quad (2.13)$$

Equation (2.13) provides an "exact" form of the transport for the second order velocity scalar correlations. In this equation, the production term $P_i^\alpha$, the transport term $T_{ik}^\alpha$, the dissipation term $\epsilon_i^\alpha$ and the pressure-rate-of-scalar-strain $\Pi_i^\alpha$ are defined as

$$P_i^\alpha = -\tau_L(u_i,u_k)\frac{\partial \langle\phi_\alpha\rangle_L}{\partial x_k} - \tau_L(\phi_\alpha,u_k)\frac{\partial \langle u_i\rangle_L}{\partial x_k}, \quad (2.14a)$$

$$T_{ik}^\alpha = \langle\rho\rangle_\ell \tau_L(u_i,\phi_\alpha,u_k) + \tau(p,\phi_\alpha)\delta_{ik} - (\tau(\phi_\alpha,\tau_{ik}) - \tau(u_i,J_k^\alpha)), \quad (2.14b)$$

$$\epsilon_i^\alpha = \left(\left\langle \tau_{ik}\frac{\partial \phi_\alpha}{\partial x_k}\right\rangle_\ell - \breve{\tau}_{ik}\frac{\partial \langle\phi_\alpha\rangle_L}{\partial x_k}\right) - \left(\left\langle J_k^\alpha \frac{\partial u_i}{\partial x_k}\right\rangle_\ell - \breve{J}_k^\alpha \frac{\partial \langle u_i\rangle_L}{\partial x_k}\right), \quad (2.14c)$$

$$\Pi_i^\alpha = \left\langle p\frac{\partial \phi_\alpha}{\partial x_i}\right\rangle_\ell - \langle p\rangle_\ell \frac{\partial \langle\phi_\alpha\rangle_L}{\partial x_i}. \quad (2.14d)$$

In Eq. (2.14b), the subgrid terms without the subscript are defined as:

$$\tau(p,\phi_\alpha) = \langle p\phi_\alpha\rangle_\ell - \langle p\rangle_\ell \langle\phi_\alpha\rangle_L, \quad (2.15a)$$

$$\tau(\phi_\alpha,\tau_{ik}) = \langle\phi_\alpha\tau_{ik}\rangle_\ell - \langle\phi_\alpha\rangle_L \breve{\tau}_{ik}, \quad (2.15b)$$

$$\tau(u_i,J_k^\alpha) = \langle u_i J_k^\alpha\rangle_\ell - \langle u_i\rangle_L \breve{J}_k^\alpha. \quad (2.15c)$$

The second order velocity-energy correlations are governed by

$$\begin{aligned}\frac{\partial \langle\rho\rangle_\ell \tau_L(u_i,e)}{\partial t}+\frac{\partial \langle\rho\rangle_\ell \langle u_k\rangle_L \tau_L(u_i,e)}{\partial x_k} &= \langle\rho\rangle_\ell P_i^e-\frac{\partial T_{ik}^e}{\partial x_k}-\epsilon_i^e+\Pi_i^e \\ &+\left(\left\langle u_i\tau_{kj}\frac{\partial u_k}{\partial x_j}\right\rangle_\ell-\langle u_i\rangle_L\left\langle \tau_{kj}\frac{\partial u_k}{\partial x_j}\right\rangle_\ell\right) \\ &-\left(\left\langle u_i p\frac{\partial u_j}{\partial x_j}\right\rangle_\ell-\langle u_i\rangle_L\left\langle p\frac{\partial u_j}{\partial x_j}\right\rangle_\ell\right). \quad (2.16)\end{aligned}$$

Equation (2.16) provides an "exact" form of the transport for the second order velocity-energy correlations. In this equation, the production term $P_i^e$, the transport term $T_{ik}^e$, the dissipation term $\epsilon_i^e$ and the pressure-rate-of-scalar-strain $\Pi_i^e$ are defined as

$$P_i^e = -\tau_L(u_i,u_k)\frac{\partial \langle e\rangle_L}{\partial x_k}-\tau_L(e,u_k)\frac{\partial \langle u_i\rangle_L}{\partial x_k}, \quad (2.17a)$$

$$T_{ik}^e = \langle\rho\rangle_\ell \tau_L(u_i,e,u_k)+\tau(p,e)\delta_{ik}-(\tau(e,\tau_{ik})-\tau(u_i,q_k)), \quad (2.17b)$$

$$\epsilon_i^e = \left(\left\langle \tau_{ik}\frac{\partial e}{\partial x_k}\right\rangle_\ell-\breve{\tau}_{ik}\frac{\partial \langle e\rangle_L}{\partial x_k}\right)-\left(\left\langle q_k\frac{\partial u_i}{\partial x_k}\right\rangle_\ell-\breve{q}_k\frac{\partial \langle u_i\rangle_L}{\partial x_k}\right), \quad (2.17c)$$

$$\Pi_i^e = \left\langle p\frac{\partial e}{\partial x_i}\right\rangle_\ell-\langle p\rangle_\ell\frac{\partial \langle e\rangle_L}{\partial x_i}. \quad (2.17d)$$

In Eq. (2.17b), the subgrid terms without the subscript are defined as

$$\tau(p,e) = \langle pe\rangle_\ell-\langle p\rangle_\ell\langle e\rangle_L, \quad (2.18a)$$

$$\tau(e,\tau_{ik}) = \langle e\tau_{ik}\rangle_\ell-\langle e\rangle_L\breve{\tau}_{ik}, \quad (2.18b)$$

$$\tau(u_i,q_k) = \langle u_iq_k\rangle_\ell-\langle u_i\rangle_L\breve{q}_k. \quad (2.18c)$$

The second order energy correlations are governed by

$$\begin{aligned}\frac{\partial \langle\rho\rangle_\ell \frac{\tau_L(e,e)}{2}}{\partial t} + \frac{\partial \langle\rho\rangle_\ell \langle u_k\rangle_L \frac{\tau_L(e,e)}{2}}{\partial x_k} &= \langle\rho\rangle_\ell P^{ee} - \frac{1}{2}\frac{\partial T_k^{ee}}{\partial x_k} - \epsilon^{ee} \\ &+ \left(\left\langle e\tau_{ij}\frac{\partial u_i}{\partial x_j}\right\rangle_\ell - \langle e\rangle_L \left\langle \tau_{ij}\frac{\partial u_i}{\partial x_j}\right\rangle_\ell\right) \\ &- \left(\left\langle ep\frac{\partial u_j}{\partial x_j}\right\rangle_\ell - \langle e\rangle_L \left\langle p\frac{\partial u_j}{\partial x_j}\right\rangle_\ell\right). \end{aligned} \tag{2.19}$$

Equation (2.19) provides an "exact" form of the transport for the second order energy correlations. In this equation, the production term $P^{ee}$, the transport term $T_k^{ee}$ and the dissipation term $\epsilon^{ee}$ are defined as

$$P^{ee} = -\tau_L\left(e, u_k\right)\frac{\partial \langle e\rangle_L}{\partial x_k}, \tag{2.20a}$$

$$T_k^{ee} = \langle\rho\rangle_\ell \tau_L\left(e, e, u_k\right) + 2\tau\left(e, q_k\right), \tag{2.20b}$$

$$\epsilon^{ee} = -\left(\left\langle q_k\frac{\partial e}{\partial x_k}\right\rangle_\ell - \breve{q}_k\frac{\partial \langle e\rangle_L}{\partial x_k}\right). \tag{2.20c}$$

In Eq. (2.20b), the subgrid term without the subscript is defined as

$$\tau\left(e, q_k\right) = \langle eq_k\rangle_\ell - \langle e\rangle_L \breve{q}_k. \tag{2.21}$$

The second order pressure correlations are governed by

$$\frac{\partial \frac{\tau_\ell(p,p)}{2}}{\partial t} + \frac{\partial \langle u_k \rangle_\ell \frac{\tau_\ell(p,p)}{2}}{\partial x_k} = P^{pp} - \frac{1}{2}\frac{\partial T_k^{pp}}{\partial x_k} + \epsilon^{pp} - \frac{(2\gamma-1)}{2}\tau_\ell(p,p)\frac{\partial \langle u_k \rangle_\ell}{\partial x_k}$$

$$- \gamma \langle p \rangle_\ell \Pi_d$$

$$- \frac{(2\gamma-1)}{2}\tau_\ell\left(p^2, \frac{\partial u_k}{\partial x_k}\right) - \langle p \rangle_\ell \tau_\ell\left(p, \frac{\partial u_k}{\partial x_k}\right). \tag{2.22}$$

Equation (2.22) provides an "exact" form of the transport equations for the second order pressure correlations. In this equation, the production term $P^{pp}$, the transport term $T_k^{pp}$ and the dissipation term $\epsilon^{pp}$ are defined as

$$P^{pp} = -\tau_\ell(p, u_k)\frac{\partial \langle p \rangle_\ell}{\partial x_k}, \tag{2.23a}$$

$$T_k^{pp} = \tau_\ell\left(p^2, u_k\right) - 2\langle p \rangle_\ell \tau_\ell(p, u_k), \tag{2.23b}$$

$$\begin{aligned} \epsilon^{pp} &= -(\gamma-1)\left[\left\langle p\frac{\partial q_j}{\partial x_j}\right\rangle_\ell - \langle p \rangle_\ell \frac{\partial \breve{q}_j}{\partial x_j}\right] \\ &+ (\gamma-1)\left[\left\langle p\tau_{ij}\frac{\partial u_i}{\partial x_j}\right\rangle_\ell - \langle p \rangle_\ell \left\langle \tau_{ij}\frac{\partial u_i}{\partial x_j}\right\rangle_\ell\right]. \end{aligned} \tag{2.23c}$$

The second order scalar correlations are governed by

$$\frac{\partial \langle\rho\rangle_\ell \tau_L(\phi_\alpha,\phi_\beta)}{\partial t} + \frac{\partial \langle\rho\rangle_\ell \langle u_k\rangle_L \tau_L(\phi_\alpha,\phi_\beta)}{\partial x_k} = \langle\rho\rangle_\ell P^{\alpha\beta} - \frac{\partial T_k^{\alpha\beta}}{\partial x_k} - \epsilon^{\alpha\beta}. \tag{2.24}$$

Equation (2.24) provides an "exact" form of the transport for the second order scalar correlations. In this equation, the production term $P^{\alpha\beta}$, the transport term $T_k^{\alpha\beta}$, and the dissipation term $\epsilon^{\alpha\beta}$ are defined as

$$P^{\alpha\beta} = -\tau_L(\phi_\alpha,u_k)\frac{\partial \langle\phi_\beta\rangle_L}{\partial x_k} - \tau_L(\phi_\beta,u_k)\frac{\partial \langle\phi_\alpha\rangle_L}{\partial x_k}, \tag{2.25a}$$

$$T_k^{\alpha\beta} = \langle\rho\rangle_\ell \tau_L(\phi_\alpha,\phi_\beta,u_k) - \langle\rho\rangle_\ell \Gamma\frac{\partial \tau_L(\phi_\alpha,\phi_\beta)}{\partial x_k}, \tag{2.25b}$$

$$\epsilon^{\alpha\beta} = 2\langle\rho\rangle_\ell \Gamma\tau_L\left(\frac{\partial\phi_\alpha}{\partial x_j},\frac{\partial\phi_\beta}{\partial x_j}\right). \tag{2.25c}$$

## 2.3 EXACT PEVC-FMDF TRANSPORT EQUATION

The "pressure-energy-velocity-composition filtered mass density function" (PEVC-FMDF), denoted by $P_L$, is formally defined as[20]

$$P_L\left(\boldsymbol{v},\boldsymbol{\psi},\theta,\eta,\mathbf{x};t\right)=\int_{-\infty}^{+\infty}\rho(\mathbf{x}',t)\zeta\Big(\boldsymbol{v},\boldsymbol{\psi},\theta,\eta;\boldsymbol{u}(\mathbf{x}',t),\boldsymbol{\phi}(\mathbf{x}',t),$$

$$e(\mathbf{x}',t),p(\mathbf{x}',t)\Big)G(\mathbf{x}'-\mathbf{x})d\mathbf{x}', \tag{2.26}$$

where

$$\zeta\Big(\boldsymbol{v},\boldsymbol{\psi},\theta,\eta;\boldsymbol{u}(\mathbf{x},t),\boldsymbol{\phi}(\mathbf{x},t),e(\mathbf{x},t),p(\mathbf{x},t)\Big)=\left(\prod_{i=1}^{3}\delta\left(v_i-u_i(\mathbf{x},t)\right)\right)$$

$$\times\left(\prod_{\alpha=1}^{\sigma=N_s}\delta\left(\psi_\alpha-\phi_\alpha(\mathbf{x},t)\right)\right)\times\delta\left(\theta-e(\mathbf{x},t)\right)\times\delta\left(\eta-p(\mathbf{x},t)\right), \tag{2.27}$$

where $\delta$ denotes the Dirac delta function, and $\boldsymbol{v}$, $\boldsymbol{\psi}$, $\theta$ and $\eta$ are the velocity vector, the scalar array, the sensible internal energy and pressure in the sample space. The term $\zeta$ is the "fine-grained" density.[59,68] Equation (2.26) defines the PEVC-FMDF as the spatially filtered value of the fine-grained density. With the condition of a positive filter kernel,[69] $P_L$ has all of the properties of a mass density function (MDF).[59] For further developments it is useful to define the "conditional filtered value" of the variable $Q(\mathbf{x},t)$ as:

$$\Big\langle Q(\mathbf{x},t)\,\Big|\,\boldsymbol{u}(\mathbf{x},t)=\boldsymbol{v},\boldsymbol{\phi}(\mathbf{x},t)=\boldsymbol{\psi},e(\mathbf{x},t)=\theta,p(\mathbf{x},t)=\eta\Big\rangle_L\equiv\Big\langle Q\,\Big|\,\boldsymbol{v},\boldsymbol{\psi},\theta,\eta\,\Big\rangle_L=$$

$$\frac{\int_{-\infty}^{+\infty}Q(\mathbf{x}',t)\rho(\mathbf{x}',t)\zeta\left(\boldsymbol{v},\boldsymbol{\psi},\theta,\eta;\boldsymbol{u}(\mathbf{x}',t),\boldsymbol{\phi}(\mathbf{x}',t),e(\mathbf{x}',t),p(\mathbf{x}',t)\right)G(\mathbf{x}'-\mathbf{x})d\mathbf{x}'}{P_L\left(\boldsymbol{v},\boldsymbol{\psi},\theta,\eta,\mathbf{x};t\right)}. \tag{2.28}$$

Equation (2.28) implies the following:

1. For $Q(\mathbf{x},t)=c$:

$$\Big\langle Q(\mathbf{x},t)\,\Big|\,\boldsymbol{v},\boldsymbol{\psi},\theta,\eta\Big\rangle_\ell=c, \tag{2.29}$$

   i.e., the conditional mean of a constant is the constant.

2. For $Q(\mathbf{x},t) \equiv \hat{Q}(\boldsymbol{u}(\mathbf{x},t),\boldsymbol{\phi}(\mathbf{x},t),e(\mathbf{x},t),p(\mathbf{x},t))$:

$$\left\langle Q(\mathbf{x},t) \,\middle|\, \boldsymbol{v},\boldsymbol{\psi},\theta,\eta \right\rangle_{\ell} = \hat{Q}(\boldsymbol{v},\boldsymbol{\psi},\theta,\eta), \tag{2.30}$$

i.e., the conditional mean of a known function of the dependent variables is simply the function evaluated based on the conditioning (sample-space) variables.

3. Integral properties:

$$\langle \rho(\mathbf{x},t) Q(\mathbf{x},t) \rangle_{\ell} = \int_{-\infty}^{+\infty} \int_{-\infty}^{+\infty} \left\langle Q(\mathbf{x},t) \,\middle|\, \boldsymbol{v},\boldsymbol{\psi},\theta,\eta \right\rangle_{\ell} P_L(\boldsymbol{v},\boldsymbol{\psi},\theta,\eta,\mathbf{x};t) d\boldsymbol{v} d\boldsymbol{\psi} d\theta d\eta, \tag{2.31}$$

i.e., the probability weighted mean of the conditional mean is the unconditional mean.

From Eqs. (2.29), (2.30), and (2.31) it follows that the filtered value of any function of the velocity and/or scalar variables is obtained by its integration over the sample spaces:

$$\langle \rho(\mathbf{x},t) \rangle_{\ell} \langle Q(\mathbf{x},t) \rangle_{L} = \int_{-\infty}^{+\infty} \int_{-\infty}^{+\infty} \hat{Q}(\boldsymbol{v},\boldsymbol{\psi},\theta,\eta) P_L(\boldsymbol{v},\boldsymbol{\psi},\theta,\eta,\mathbf{x};t) d\boldsymbol{v} d\boldsymbol{\psi} d\theta d\eta. \tag{2.32}$$

The exact transport equation for the PEVC-FMDF is derived by starting with the time derivative of the fine-grained density function [Eq. (2.27)]:

$$\frac{\partial \zeta}{\partial t} = -\left( \frac{\partial u_k}{\partial t}\frac{\partial \zeta}{\partial \boldsymbol{v}_k} + \frac{\partial \phi_\alpha}{\partial t}\frac{\partial \zeta}{\partial \boldsymbol{\psi}_\alpha} + \frac{\partial e}{\partial t}\frac{\partial \zeta}{\partial \theta} + \frac{\partial p}{\partial t}\frac{\partial \zeta}{\partial \eta} \right). \tag{2.33}$$

Substituting Eqs. (2.1) and (2.4), into Eq. (2.33) yields

$$\begin{aligned} \frac{\partial \rho\zeta}{\partial t} + \frac{\partial \rho u_j \zeta}{\partial x_j} &= \left( \frac{\partial p}{\partial x_j} - \frac{\partial \tau_{kj}}{\partial x_k} \right) \frac{\partial \zeta}{\partial \boldsymbol{v}_j} + \left( \frac{\partial J_j^\alpha}{\partial x_j} \right) \frac{\partial \zeta}{\partial \boldsymbol{\psi}_\alpha} \\ &+ \left( \gamma \rho p \frac{\partial u_j}{\partial x_j} + (\gamma - 1)\, \rho \frac{\partial q_i}{\partial x_i} - (\gamma - 1)\, \rho \tau_{ij} \frac{\partial u_i}{\partial x_j} \right) \frac{\partial \zeta}{\partial \eta} \\ &+ \left( \frac{\partial q_i}{\partial x_i} - \tau_{ij} \frac{\partial u_i}{\partial x_j} + p \frac{\partial u_j}{\partial x_j} \right) \frac{\partial \zeta}{\partial \theta}. \end{aligned} \tag{2.34}$$

Integration of this equation according to Eq. (2.26), while employing Eq. (2.28) results in

$$
\begin{aligned}
\frac{\partial P_L}{\partial t}+\frac{\partial \boldsymbol{v}_j P_L}{\partial x_j} &= \frac{\partial}{\partial \boldsymbol{v}_i}\left(\left\langle \frac{1}{\rho}\frac{\partial p}{\partial x_i}\,\middle|\,\boldsymbol{v},\boldsymbol{\psi},\theta,\eta\right\rangle_{\ell} P_L\right)\\
&- \frac{\partial}{\partial \boldsymbol{v}_i}\left(\left\langle \frac{1}{\rho}\frac{\partial \tau_{ij}}{\partial x_j}\,\middle|\,\boldsymbol{v},\boldsymbol{\psi},\theta,\eta\right\rangle_{\ell} P_L\right)\\
&+ \frac{\partial}{\partial \psi_\alpha}\left(\left\langle \frac{1}{\rho}\frac{\partial J_j^\alpha}{\partial x_j}\,\middle|\,\boldsymbol{v},\boldsymbol{\psi},\theta,\eta\right\rangle_{\ell} P_L\right)\\
&+ \frac{\partial}{\partial \theta}\left(\left\langle \frac{1}{\rho}\frac{\partial q_i}{\partial x_i}\,\middle|\,\boldsymbol{v},\boldsymbol{\psi},\theta,\eta\right\rangle_{\ell} P_L\right)\\
&- \frac{\partial}{\partial \theta}\left(\left\langle \frac{1}{\rho}\tau_{ij}\frac{\partial u_i}{\partial x_j}\,\middle|\,\boldsymbol{v},\boldsymbol{\psi},\theta,\eta\right\rangle_{\ell} P_L\right)\\
&+ \frac{\partial}{\partial \theta}\left(\left\langle \frac{1}{\rho}p\frac{\partial u_j}{\partial x_j}\,\middle|\,\boldsymbol{v},\boldsymbol{\psi},\theta,\eta\right\rangle_{\ell} P_L\right)\\
&+ (\gamma-1)\frac{\partial}{\partial \eta}\left(\left\langle \frac{\partial q_i}{\partial x_i}\,\middle|\,\boldsymbol{v},\boldsymbol{\psi},\theta,\eta\right\rangle_{\ell} P_L\right)\\
&- (\gamma-1)\frac{\partial}{\partial \eta}\left(\left\langle \tau_{ij}\frac{\partial u_i}{\partial x_j}\,\middle|\,\boldsymbol{v},\boldsymbol{\psi},\theta,\eta\right\rangle_{\ell} P_L\right)\\
&+ \gamma\frac{\partial}{\partial \eta}\left(\left\langle p\frac{\partial u_j}{\partial x_j}\,\middle|\,\boldsymbol{v},\boldsymbol{\psi},\theta,\eta\right\rangle_{\ell} P_L\right). \qquad (2.35)
\end{aligned}
$$

This is an exact PEVC-FMDF transport equation in which the effect of convection appears in closed form. The conditional terms at the right hand side are unclosed.

## 2.4 MODELED PEVC-FMDF TRANSPORT EQUATION

To develop the model for the PEVC-FMDF, the notion of "stochastic" particles[62] is used. This is via development of SDEs governing the FDF transport variables: $U_i^+$, $\phi_\alpha^+$, $E^+$, and $P^+$. The internal energy is modeled according to the first law of thermodynamics:

$$dE^+ = \Big( - C_e\Omega \left[E^+ - \langle e \rangle_L\right] + \frac{E^+(\gamma-1)}{P^+}\epsilon\Big)dt - P^+ d\xi^+, \tag{2.36}$$

where $C_e$ is the model constant, $\Omega$ denotes the SGS mixing frequency, and $\xi^+ = 1/\rho^+$ is the specific volume relating $E^+$ and $P^+$ through the equation of state. In the context of single-point formulation both of these variables need closures. In the absence of better alternatives, the simple models suggested in the previous work[9] are adopted:

$$\epsilon = \langle \rho \rangle_\ell \, C_\epsilon k^{3/2}/\Delta_L, \tag{2.37a}$$

$$\Omega = \epsilon/(\langle \rho \rangle_\ell \, k), \tag{2.37b}$$

here $C_\epsilon$ is the model constant, $\Delta_L$ is the LES filter size and $k = \frac{1}{2}\,\tau_L\,(u_i, u_i)$ is the SGS kinetic energy. The pressure SDE is written in the general form

$$dP^+ = P^+ \left(A dt + B dW_p\right), \tag{2.38}$$

where $W_p(t)$ denotes the Wiener process.[70] With this, the energy SDE takes the form

$$dE^+ = \Big( - \frac{C_e\Omega}{\gamma}\left(E^+ - \langle e \rangle_L\right) + \frac{\gamma-1}{\gamma}\frac{E^+}{P^+}\epsilon + \frac{\gamma-1}{\gamma}E^+\left(A - \frac{B^2}{\gamma}\right)\Big)dt$$

$$+ \frac{\gamma-1}{\gamma}E^+ B dW_p. \tag{2.39}$$

The coefficients $A$ and $B$ are determined so that the exact and modeled transport equations for energy are identical, and the filtered specific volume is consistently determined by the

FDF and the equation of state. There are different combinations of $A$ and $B$ that satisfy these constraints. To ensure realizability, we select the model[71,72]

$$\begin{aligned} A &= \frac{\epsilon\left(\gamma-1\right)}{P^{+}}-\gamma\frac{\partial\left\langle u_j\right\rangle_{\ell}}{\partial x_j}+\varkappa_P\left(\gamma-1\right)\left(P^{+}-\left\langle p\right\rangle_{\ell}\right) \\ &+ \gamma\frac{\partial}{\partial x_j}\left(\mu\frac{\partial}{\partial x_j}\left(\frac{1}{\left\langle\rho\right\rangle_{\ell}}\right)\right), \end{aligned} \tag{2.40}$$

$$B = 0, \tag{2.41}$$

with:

$$\varkappa_P=\frac{\gamma}{\left(\gamma-1\right)\tau_{\ell}\left(p,p\right)}\left(\breve{\tau_{ij}}\frac{\partial\left\langle u_i\right\rangle_L}{\partial x_j}-\mathcal{F}_d-\left\langle p\right\rangle_{\ell}\frac{\partial}{\partial x_j}\left(\mu\frac{\partial}{\partial x_i}\left(\frac{1}{\left\langle\rho\right\rangle_{\ell}}\right)\right)\right), \tag{2.42}$$

where $\mathcal{F}_d$ is the general form of the model for the pressure dilatation based on known SGS statistics. For modeling of the other variables, we follow Refs.[12,18,23,73,74] and use the simplified Langevin model (SLM) and linear mean-square estimation (LMSE) model[75]

$$d{X_i}^{+}=U_i^{+}dt+\sqrt{\frac{2\mu}{\left\langle\rho\right\rangle_{\ell}}}dW_i, \tag{2.43a}$$

$$\begin{aligned} dU_i^{+} &= -\frac{1}{\left\langle\rho\right\rangle_{\ell}}\frac{\partial\left\langle p\right\rangle_{\ell}}{\partial x_i}dt+\frac{2}{\left\langle\rho\right\rangle_{\ell}}\frac{\partial}{\partial x_j}\left(\mu\frac{\partial\left\langle u_i\right\rangle_L}{\partial x_j}\right)dt+\frac{1}{\left\langle\rho\right\rangle_{\ell}}\frac{\partial}{\partial x_j}\left(\mu\frac{\partial\left\langle u_j\right\rangle_L}{\partial x_i}\right)dt \\ &- \frac{2}{3}\frac{1}{\left\langle\rho\right\rangle_{\ell}}\frac{\partial}{\partial x_i}\left(\mu\frac{\partial\left\langle u_j\right\rangle_L}{\partial x_j}\right)dt+G_{ij}\left(U_j^{+}-\left\langle u_j\right\rangle_L\right)dt+\sqrt{C_0\frac{\epsilon}{\left\langle\rho\right\rangle_{\ell}}}dW_i' \\ &+ \sqrt{\frac{2\mu}{\left\langle\rho\right\rangle_{\ell}}}\frac{\partial\left\langle u_i\right\rangle_L}{\partial x_j}dW_j, \end{aligned} \tag{2.43b}$$

$$d\phi_{\alpha}^{+}=-C_{\phi}\Omega\left(\phi_{\alpha}^{+}-\left\langle\phi_{\alpha}\right\rangle_L\right)dt, \tag{2.43c}$$

where $\mathbf{W}$, $\mathbf{W}'$ denote the Wiener process in the physical and the velocity spaces, respectively, and

$$G_{ij} = \left( \frac{\Pi_d}{2k \langle \rho \rangle_\ell} - \Omega \left( \frac{1}{2} + \frac{3}{4} C_0 \right) \right) \delta_{ij}, \tag{2.44}$$

in which we employ the model

$$\Pi_d = C_\Pi \left( \left\langle \langle p \rangle_\ell \frac{\partial \langle u_i \rangle_\ell}{\partial x_i} \right\rangle_{\ell_2} - \langle \langle p \rangle_\ell \rangle_{\ell_2} \frac{\partial \langle \langle u_i \rangle_\ell \rangle_{\ell_2}}{\partial x_i} \right). \tag{2.45}$$

The parameters $C_0$, $C_\phi$, and $C_\Pi$ are the model constants and needed to be specified.[11,76] The Fokker-Planck equation,[77] governing the joint probability density function of the SGS transport parameters is

$$\begin{aligned}
\frac{\partial F_L}{\partial t} + \frac{\partial v_i F_L}{\partial x_i} = {} & \frac{1}{\langle \rho \rangle_\ell} \frac{\partial \langle p \rangle_\ell}{\partial x_i} \frac{\partial F_L}{\partial v_i} - \frac{2}{\langle \rho \rangle_\ell} \frac{\partial}{\partial x_j} \left( \mu \frac{\partial \langle u_i \rangle_L}{\partial x_j} \right) \frac{\partial F_L}{\partial v_i} - \frac{1}{\langle \rho \rangle_\ell} \frac{\partial}{\partial x_j} \left( \mu \frac{\partial \langle u_j \rangle_L}{\partial x_i} \right) \frac{\partial F_L}{\partial v_i} \\
& + \frac{2}{3} \frac{1}{\langle \rho \rangle_\ell} \frac{\partial}{\partial x_i} \left( \mu \frac{\partial \langle u_j \rangle_L}{\partial x_j} \right) \frac{\partial F_L}{\partial v_i} - \frac{\partial \left( G_{ij} \left( v_j - \langle u_j \rangle_L \right) F_L \right)}{\partial v_i} + \frac{\partial}{\partial x_i} \left( \mu \frac{\partial (F_L / \langle \rho \rangle_\ell)}{\partial x_i} \right) \\
& + \frac{\partial}{\partial x_i} \left( \frac{2\mu}{\langle \rho \rangle_\ell} \frac{\partial \langle u_j \rangle_L}{\partial x_i} \frac{\partial F_L}{\partial v_j} \right) + \frac{\mu}{\langle \rho \rangle_\ell} \frac{\partial \langle u_k \rangle_L}{\partial x_j} \frac{\partial \langle u_i \rangle_L}{\partial x_j} \frac{\partial^2 F_L}{\partial v_k \partial v_i} + \frac{1}{2} C_0 \frac{\epsilon}{\langle \rho \rangle_\ell} \frac{\partial^2 F_L}{\partial v_i \partial v_i} \\
& + C_\phi \Omega \frac{\partial \left( \left( \psi_\alpha - \langle \phi_\alpha \rangle_L \right) F_L \right)}{\partial \psi_\alpha} + \frac{C_e \Omega}{\gamma} \frac{\partial \left( \left( \theta - \langle e \rangle_L \right) F_L \right)}{\partial \theta} - \frac{\gamma - 1}{\gamma} (\epsilon) \frac{\partial}{\partial \theta} \left( \frac{\theta}{\eta} F_L \right) \\
& - \frac{\gamma - 1}{\gamma} \frac{\partial \left( \theta A F_L \right)}{\partial \theta} + \frac{\gamma - 1}{\gamma^2} \frac{\partial \left( \theta B^2 F_L \right)}{\partial \theta} - \frac{\partial \left( \eta A F_L \right)}{\partial \eta} + \frac{1}{2} \frac{(\gamma - 1)^2}{\gamma^2} \frac{\partial^2 \left( \theta^2 B^2 F_L \right)}{\partial \theta \partial \theta} \\
& + \frac{\gamma - 1}{\gamma} \frac{\partial^2 \left( \theta \eta B^2 F_L \right)}{\partial \theta \partial \eta} + \frac{1}{2} \frac{\partial^2 \left( \eta^2 B^2 F_L \right)}{\partial \eta \partial \eta}.
\end{aligned} \tag{2.46}$$

The transport equations for the first-order moments are obtained by integration of Eq. (2.46) according to Eq. (2.32)

$$\frac{\partial \langle\rho\rangle_\ell}{\partial t} + \frac{\partial \langle\rho\rangle_\ell \langle u_j\rangle_L}{\partial x_j} = 0, \tag{2.47a}$$

$$\frac{\partial \langle\rho\rangle_\ell \langle u_i\rangle_L}{\partial t} + \frac{\partial \langle\rho\rangle_\ell \langle u_j\rangle_L \langle u_i\rangle_L}{\partial x_j} = -\frac{\partial \langle p\rangle_\ell}{\partial x_i} + \frac{\partial \breve{\tau}_{ij}}{\partial x_j} - \frac{\partial \langle\rho\rangle_\ell \tau_L(u_i,u_j)}{\partial x_j}, \tag{2.47b}$$

$$\begin{aligned}\frac{\partial \langle\rho\rangle_\ell \langle e\rangle_L}{\partial t} + \frac{\partial \langle\rho\rangle_\ell \langle u_j\rangle_L \langle e\rangle_L}{\partial x_j} &= \frac{\partial}{\partial x_j}\left(\mu \frac{\partial \langle e\rangle_L}{\partial x_j}\right) - \frac{\partial \langle\rho\rangle_\ell \tau_L(e,u_j)}{\partial x_j} \\ &+ \epsilon + \breve{\tau}_{ij}\frac{\partial \langle u_i\rangle_L}{\partial x_j} - \Pi_d - \langle p\rangle_\ell \frac{\partial \langle u_i\rangle_\ell}{\partial x_i},\end{aligned} \tag{2.47c}$$

$$\frac{\partial \langle\rho\rangle_\ell \langle\phi_\alpha\rangle_L}{\partial t} + \frac{\partial \langle\rho\rangle_\ell \langle u_j\rangle_L \langle\phi_\alpha\rangle_L}{\partial x_j} = \frac{\partial}{\partial x_j}\left(\mu \frac{\partial \langle\phi_\alpha\rangle_L}{\partial x_j}\right) - \frac{\partial \langle\rho\rangle_\ell \tau_L(\phi_\alpha,u_j)}{\partial x_j}, \tag{2.47d}$$

$$\begin{aligned}\frac{\partial \langle p\rangle_\ell}{\partial t} + \frac{\partial \langle p\rangle_\ell \langle u_j\rangle_\ell}{\partial x_j} &= (\gamma-1)\frac{\partial}{\partial x_j}\left(\mu \frac{\partial \langle e\rangle_L}{\partial x_j}\right) - \frac{\partial \tau_\ell(p,u_j)}{\partial x_j} \\ &+ (\gamma-1)\,\epsilon + (\gamma-1)\,\breve{\tau}_{ij}\frac{\partial \langle u_i\rangle_L}{\partial x_j} \\ &- (\gamma-1)\,\Pi_d - (\gamma-1)\,\langle p\rangle_\ell \frac{\partial \langle u_i\rangle_\ell}{\partial x_i}.\end{aligned} \tag{2.47e}$$

The set of Eqs. (2.47) are identical to Eq. (2.7). The transport equations for the second order correlations are obtained by integration of Eq. (2.46) according to Eq. (2.32)

$$\frac{\partial \langle\rho\rangle_\ell \tau_L(u_i,u_j)}{\partial t} + \frac{\partial \langle\rho\rangle_\ell \langle u_k\rangle_L \tau_L(u_i,u_j)}{\partial x_k} = \langle\rho\rangle_\ell P_{ij} - \frac{\partial \langle\rho\rangle_\ell \tau_L(u_k,u_i,u_j)}{\partial x_k}$$

$$+ G_{jk}\langle\rho\rangle_\ell \tau_L(u_k,u_i) + G_{ik}\langle\rho\rangle_\ell \tau_L(u_k,u_j)$$

$$+ \frac{\partial}{\partial x_k}\left(\mu\frac{\partial \tau_L(u_i,u_j)}{\partial x_k}\right) + C_0\epsilon\delta_{ij}, \tag{2.48}$$

$$\frac{\partial \langle\rho\rangle_\ell \tau_L(u_i,\phi_\alpha)}{\partial t} + \frac{\partial \langle\rho\rangle_\ell \langle u_k\rangle_L \tau_L(u_i,\phi_\alpha)}{\partial x_k} = \langle\rho\rangle_\ell P_i^\alpha - \frac{\partial \langle\rho\rangle_\ell \tau_L(u_k,u_i,\phi_\alpha)}{\partial x_k}$$

$$+ \frac{\partial}{\partial x_k}\left(\mu\frac{\partial \tau_L(u_i,\phi_\alpha)}{\partial x_k}\right) + G_{ik}\langle\rho\rangle_\ell \tau_L(u_k,\phi_\alpha)$$

$$- C_\phi\Omega\langle\rho\rangle_\ell \tau_L(u_i,\phi_\alpha), \tag{2.49}$$

$$\frac{\partial \langle\rho\rangle_\ell \tau_L(u_i,e)}{\partial t} + \frac{\partial \langle\rho\rangle_\ell \langle u_k\rangle_L \tau_L(u_i,e)}{\partial x_k} = \langle\rho\rangle_\ell P_i^e - \frac{\partial \langle\rho\rangle_\ell \tau_L(u_k,u_i,e)}{\partial x_k}$$

$$+ \frac{\partial}{\partial x_k}\left(\mu\frac{\partial \tau_L(u_i,e)}{\partial x_k}\right) + G_{ik}\langle\rho\rangle_\ell \tau_L(u_k,e) - \frac{C_e\Omega}{\gamma}\langle\rho\rangle_\ell \tau_L(u_i,e)$$

$$+ \tau_\ell(p,u_i)\left[\frac{\partial}{\partial x_k}\left(\mu\frac{\partial}{\partial x_k}\left(\frac{1}{\langle\rho\rangle_\ell}\right)\right) - \frac{\partial \langle u_k\rangle_\ell}{\partial x_k}\right]$$

$$+ \left[\tau_\ell\left(p^2,u_i\right) + \langle p\rangle_\ell \tau_\ell(p,u_i)\right]\varkappa_P\frac{\gamma-1}{\gamma}\tau_\ell(p,p), \tag{2.50}$$

$$\frac{\partial \langle\rho\rangle_\ell \frac{\tau_L(e,e)}{2}}{\partial t} + \frac{\partial \langle\rho\rangle_\ell \langle u_k\rangle_L \frac{\tau_L(e,e)}{2}}{\partial x_k} = \langle\rho\rangle_\ell P^{ee} - \frac{1}{2}\frac{\partial \langle\rho\rangle_\ell \tau_L(u_k,e,e)}{\partial x_k}$$

$$+ \frac{\partial}{\partial x_k}\left(\mu\frac{\partial}{\partial x_k}\left(\frac{\tau_L(e,e)}{2}\right)\right) + \mu\frac{\partial \langle e\rangle_L}{\partial x_k}\frac{\partial \langle e\rangle_L}{\partial x_k} - \frac{C_e\Omega}{\gamma}\langle\rho\rangle_\ell \tau_L(e,e)$$

$$+ \frac{\tau(p,e)}{2}\left[\frac{\partial}{\partial x_k}\left(\mu\frac{\partial}{\partial x_k}\left(\frac{1}{\langle\rho\rangle_\ell}\right)\right) - \frac{\partial \langle u_k\rangle_\ell}{\partial x_k}\right]$$

$$+ \frac{\varkappa_P(\gamma-1)}{\gamma}\left[\tau_\ell\left(p^2,e\right) - \langle p\rangle_\ell \tau_\ell(p,e)\right], \tag{2.51}$$

$$\frac{\partial \frac{\tau_\ell(p,p)}{2}}{\partial t} + \frac{\partial \langle u_k\rangle_\ell \frac{\tau_\ell(p,p)}{2}}{\partial x_k} = P^{pp} - \frac{1}{2}\frac{\partial T_k^{pp}}{\partial x_k} - \frac{(2\gamma-1)}{2}\tau_\ell(p,p)\frac{\partial \langle u_k\rangle_\ell}{\partial x_k} - \gamma\langle p\rangle_\ell \Pi_d$$

$$+ \frac{1}{2}\frac{\partial}{\partial x_k}\Big(\mu\frac{\partial}{\partial x_k}\left(\frac{\tau_\ell(p,p)}{\langle\rho\rangle_\ell}\right)\Big)$$

$$+ \gamma\langle p\rangle_\ell \breve{\tau_{ij}}\frac{\langle u_i\rangle_L}{\partial x_j} + \frac{(2\gamma-1)}{2}\tau_\ell(p,p)\frac{\partial}{\partial x_k}\Big(\mu\frac{\partial}{\partial x_k}\left(\frac{1}{\langle\rho\rangle_\ell}\right)\Big)$$

$$+ \gamma(\gamma-1)\Big[-\langle p\rangle_\ell \frac{\partial}{\partial x_k}\left(\mu\frac{\partial \langle e\rangle_L}{\partial x_k}\right) + \langle e\rangle_L \frac{\partial}{\partial x_k}\left(\mu\frac{\partial \langle p\rangle_\ell}{\partial x_k}\right)$$

$$+ 2\mu\frac{\partial \langle e\rangle_L}{\partial x_k}\frac{\partial \langle p\rangle_\ell}{\partial x_k}\Big] - \frac{2\gamma-1}{\langle\rho\rangle_\ell}\mu\frac{\partial \langle p\rangle_\ell}{\partial x_k}\frac{\partial \langle p\rangle_\ell}{\partial x_k}, \tag{2.52}$$

$$\frac{\partial \langle\rho\rangle_\ell \tau_L(\phi_\alpha,\phi_\beta)}{\partial t} + \frac{\partial \langle\rho\rangle_\ell \langle u_k\rangle_L \tau_L(\phi_\alpha,\phi_\beta)}{\partial x_k} = \langle\rho\rangle_\ell P^{\alpha\beta} - \frac{\partial \langle\rho\rangle_\ell \tau_L(u_k,\phi_\alpha,\phi_\beta)}{\partial x_k}$$

$$+ 2\mu\frac{\partial \langle\phi_\alpha\rangle_L}{\partial x_k}\frac{\partial \langle\phi_\beta\rangle_L}{\partial x_k} + \frac{\partial}{\partial x_k}\left(\mu\frac{\partial \tau_L(\phi_\alpha,\phi_\beta)}{\partial x_k}\right) - 2C_\phi\Omega\langle\rho\rangle_\ell \tau_L(\phi_\alpha,\phi_\beta). \tag{2.53}$$

# 3.0 NUMERICAL PROCEDURE

The modeled PEVC-FMDF transport equation is solved by a hybrid finite-difference (FD) / Monte Carlo (MC) method, similar to those in previous works.[3,78] The FDF is represented by an ensemble of MC particles, each carrying the information pertaining to its position $\mathbf{X}^+$, velocity $\boldsymbol{U}^+$, composition $\boldsymbol{\phi}^+$, energy $E^+$, and pressure $P^+$. We define the $\boldsymbol{Z}^+(t)$, a $8+N_s$ vector, as:

$$\boldsymbol{Z}^+(t) = [\mathbf{X}^+(t), \boldsymbol{U}^+(t), \boldsymbol{\phi}^+(t), E^+(t), P^+(t)], \tag{3.1}$$

which evolves by:

$$d\boldsymbol{Z}^+ = \boldsymbol{D}(\boldsymbol{Z}^+)dt + \boldsymbol{B}(\boldsymbol{Z}^+)d\boldsymbol{W}, \tag{3.2}$$

where $\boldsymbol{W}$ is the Wiener-Levy vector, and the matrices $\boldsymbol{D}$ and $\boldsymbol{B}$ can be identified from Eqs. (2.36),(2.38), and (2.43). The vector $\boldsymbol{Z}$ is updated via the Euler-Maruyama discretization:[79]

$$\boldsymbol{Z}^+(t_{k+1}) = \boldsymbol{Z}^+(t_k) + \boldsymbol{D}\left(\boldsymbol{Z}^+(t_k)\right)\Delta t + \boldsymbol{B}\left(\boldsymbol{Z}^+(t_k)\right)\Delta t^{1/2}\zeta_k, \tag{3.3}$$

where $\zeta_k$ is an independent standardized Gaussian random variable at time $t_k$, and $\Delta t$ is the time step. This scheme preserves the Markovian character of the diffusion processes and the Itô-Gikhman character of the SDEs.[80]

The computational domain is discretized on equally-spaced FD grid points. These are used to identify the regions where the statistical information are to be obtained, and to perform complementary LES solely by FD discretization. The latter is referred to as LES-FD and is useful for assessing the consistency of the MC solver. In this solver, the statistical information is obtained by considering an ensemble of $N_E$ MC particles residing within a cubic domain of side $\Delta_E$ centered around each of the FD points. For reliable statistics with

minimal numerical dispersion, it is desired to minimize the size of the ensemble domain and maximize the number of the MC particles.[59] In this way:

$$\begin{aligned} \langle a \rangle_E &\equiv \frac{\sum_{n\in\Delta_E} w^{(n)} a^{(n)}}{\sum_{n\in\Delta_E} w^{(n)}} \xrightarrow[\substack{N_E\to\infty \\ \Delta_E\to 0}]{} \langle a \rangle_L \,, \\ \tau_E(a,b) &\equiv \left( \frac{\sum_{n\in\Delta_E} w^{(n)} a^{(n)} b^{(n)}}{\sum_{n\in\Delta_E} w^{(n)}} \right) - \langle a \rangle_E \langle b \rangle_E \xrightarrow[\substack{N_E\to\infty \\ \Delta_E\to 0}]{} \tau_L(a,b) \,, \end{aligned} \tag{3.4}$$

where $w^{(n)}$ is the weight of the $n^{th}$ MC particle and $a^{(n)}$ denotes the information carried by that particle pertaining to transport variable $a$. The LES-FD solver is based on the second-order predictor-corrector scheme. All of the FD operations are conducted on fixed grid points. The transfer of information from these points to the MC particles is via a trilinear interpolation. The transfer of information from the particles to the grid points is by means of ensemble averaging. The transport equations to be solved by the LES-FD include unclosed second-order moments which are obtained from the MC. The LES-FD also determines the filtered values of the transport variables. This redundancy is useful in monitoring the accuracy and consistency of the FDF results.[18,78,81]

# 4.0 RESULTS

## 4.1 FLOW AND NUMERICAL SPECIFICATIONS

Simulations are conducted of a three-dimensional (3D) temporally developing mixing layer involving the transport of a passive scalar. The temporal layer consists of two parallel streams traveling in opposite directions with the same speed.[21,82–84] The LES predictions are compared with direct numerical simulation (DNS) data of the same layer. In this layer, $x$, $y$ and $z$ denote the streamwise, the cross-stream, and the spanwise directions, respectively. The velocity components along these directions are denoted, in order, by $u$, $v$ and $w$. The transport variables are normalized with respect to the half initial vorticity thickness, $L_r = \frac{\delta_v(t=0)}{2}$. Here, $\delta_v = \frac{\Delta U}{|\partial\overline{\langle u\rangle}_L/\partial y|_{max}}$, where $\overline{\langle u\rangle}_L$ is the Reynolds-averaged value of the filtered streamwise velocity and $\Delta U$ is the velocity difference across the layer. The length $L_v$ is specified such that $L_v = 2^{N_P}\lambda_u$, where $N_P$ is the desired number of successive vortex pairings and $\lambda_u$ is the wavelength of the most unstable mode corresponding to the mean streamwise velocity profile imposed at the initial time. The normalized filtered streamwise velocity, the scalar composition and the temperature are initialized with a hyperbolic tangent profiles with $\langle u\rangle_L = 1$, $\langle\phi\rangle_L = 1$, $\langle T\rangle_L = s$ on the top stream, and $\langle u\rangle_L = -1$, $\langle\phi\rangle_L = 0$, $\langle T\rangle_L = 1$ on the bottom stream. With a constant initial pressure, the parameter "$s$" also denotes the initial density ratio across the layer; the values $s = 1,\ 2,\ 4$ are considered. The reference velocity is $U_r = \Delta U/2$. The Reynolds number is set ($Re = \frac{U_r L_r}{\nu}$) $= 50$, and the Mach numbers ($Ma = \frac{U_r}{\sqrt{\gamma R T_r}}$) values of 0.2, 0.6 and 1.2 are considered.

The 3D field is initialized in a procedure somewhat similar to that in Ref.[84] The formation of the large scale structures are expedited through eigenfunction based initial perturbations. This includes 2D and 3D perturbations with a random phase shift between the modes.

This yields the formation of two successive vortex pairings and strong three-dimensionality. Periodic boundary conditions are imposed in the homogeneous directions ($x$ and $z$), and characteristic boundary conditions[85] are employed in the cross-stream direction. Simulations are conducted on a box, $0 \leq x \leq L$, $\frac{-3L}{2} \leq y \leq \frac{3L}{2}$, $0 \leq z \leq L$ where $L = L_v/L_r$. The layer is discretized with nearly equally-spaced grid points ($\Delta y \cong \Delta x = \Delta z$) with the number of grid points $193 \times 577 \times 193$ for DNS, and $66 \times 193 \times 66$ for LES. Some lower resolution LES $33 \times 97 \times 33$ were also conducted for production runs. The resolution in LES was determined in such a way that a reasonable amount ($75\% - 85\%$) of turbulent energy is captured by the resolved scale. To filter the DNS data, a top-hat function is used with $\Delta_L = 2\,\Delta$, where $\Delta = (\Delta x \Delta y \Delta z)^{1/3}$. The LES filter sizes are $\Delta_1 = \Delta_L$ and $\Delta_2 = 2\Delta_L$. No attempt is made to investigate the sensitivity of the results to the filter function[69] or the size of the filter.[86–88]

The MC particles are initially distributed uniformly within the domain in a random fashion. The particle weights, $w^{(n)}$, are set according to filtered fluid density at the initial time. The initial number of particles per grid point is $NPG = 80$, and the ensemble domain size ($\Delta_E$) is set equal to the grid spacing. The effects of both of these parameters have been assessed in previous works.[11,18,23,24] All results are analyzed both "instantaneously" and "statistically." In the former, the instantaneous scatter plots of the variables of interest are analyzed. In the latter, the "Reynolds-averaged" statistics constructed from the instantaneous data are considered. These are constructed by spatial averaging over homogeneous directions. All Reynolds-averaged results are denoted by an overbar. No attempt is made to determine the optimum magnitudes of the model constants. The values as suggested in the literature are adopted for $C_0 = 2.1$, and $C_\phi = C_\epsilon = 1$.[11,89] The values of $C_\Pi = 1$ and $C_e = 1.4$ were chosen based on comparison with DNS data for one set of the simulations, and were used in all the subsequent ones.

## 4.2 CONSISTENCY AND VALIDITY ASSESSMENTS

To demonstrate consistency, the redundancy of the repeated fields is portrayed by scatter plots of the instantaneous values. The accuracy of the LES-FD is relatively well-established

(at least for the first-order filtered quantities), thus the comparative assessment provides a good measure of the MC performance. Sample results are given in Fig. 1, and portray a reasonable consistency.

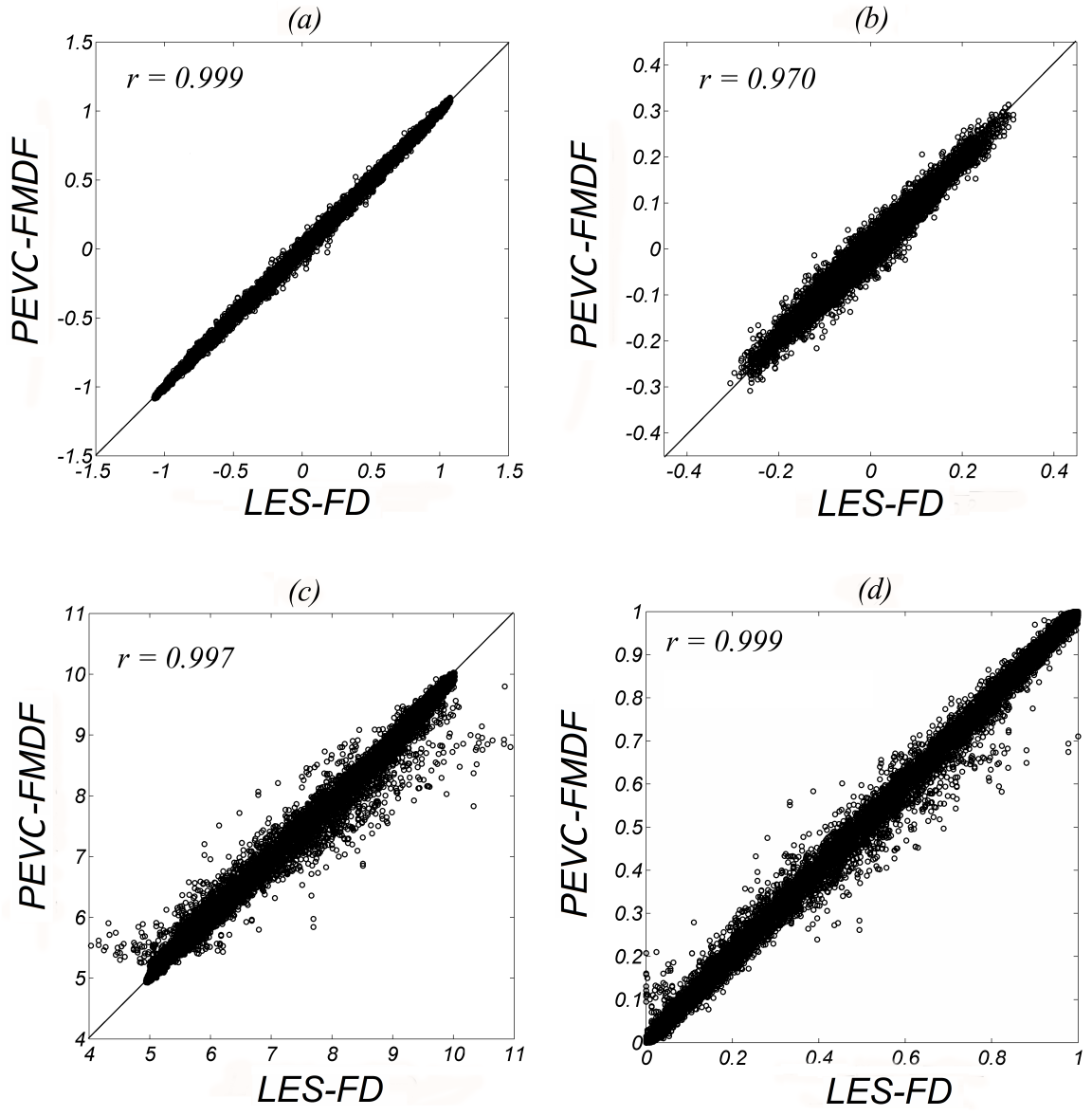


**Figure 1:** Scatter plots of (a) $\langle u \rangle_L$, (b) $\langle v \rangle_L$, (c) $\langle e \rangle_L$, and (d) $\langle \phi \rangle_L$, with $Ma = 0.6$ and $s = 2$ at $t = 45$. $r$ denotes the correlation coefficient.

For comparison with DNS data, the resolved and the "total" components of the Reynolds-averaged moments are considered. The former is denoted by $\overline{R(a,b)}$, with $R(a,b) = \left( \langle a \rangle_L - \overline{\langle a \rangle_L} \right)$

$\left(\langle b\rangle_L - \overline{\langle b\rangle_L}\right)$, and the latter by $\overline{r(a,b)}$, with $r(a,b) = (a-\overline{a})\left(b-\overline{b}\right)$; In DNS, the total components are directly available, while in LES they are approximated via $\overline{r(a,b)} \approx \overline{R(a,b)} + \overline{\tau_L(a,b)}$.[61]

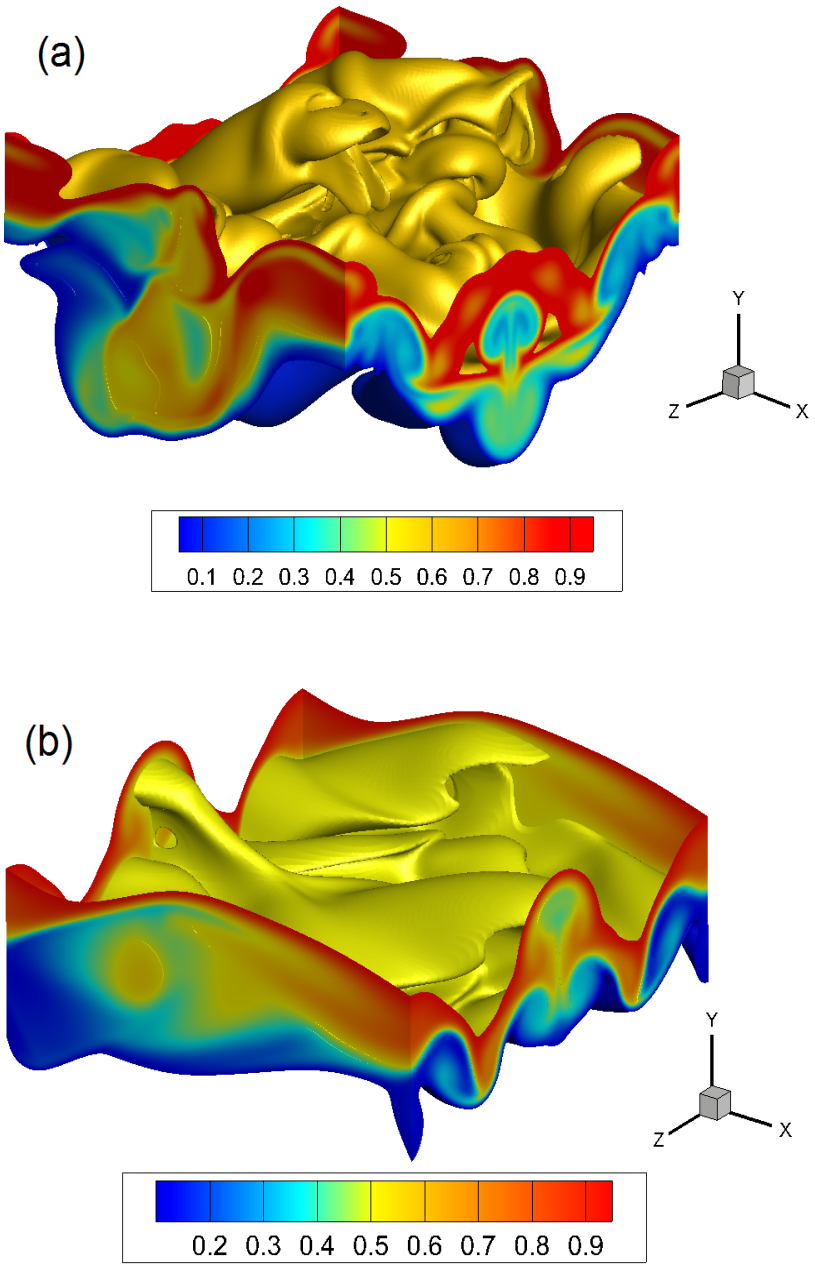


**Figure 2:** Contour surfaces of the instantaneous $\langle\phi\rangle_L$ field. (a) $Ma = 0.2$, $s = 2$ and $t = 50$, (b) $Ma = 1.2$, $s = 2$ and $t = 75$.

Figure 2 shows the instantaneous iso-surfaces of the composition field $\langle\phi\rangle_L$ obtained by PEVC-FMDF for $Ma = 0.2$ at $t = 50$ and $Ma = 1.2$ at $t = 75$. By these times, the flows have gone through pairings and exhibit strong 3D effects. This is evident by the formation of large scale spanwise rollers with the presence of secondary structures in streamwise planes.[90]

Figure 3 shows the Reynolds-averaged, filtered density and energy fields. The level of agreement between PEVC-FMDF and DNS is satisfactory. Similar agreements are observed for all other filtered variables. The figure is also indicative of the accurate prediction of shear layer center location by PEVC-FMDF. As the density ratio increases, the shear layer center, defined as the dividing mean streamline position (the position where $\overline{\langle u\rangle_L}$ is equal to the average of the free stream velocities), is shifted further to the low-density side. As a result, the peak values of the Reynolds stresses and scalar fluxes also show a shift to the low-density side. The shift is known to be responsible for the decreased correlation between density and velocity components[91] and hence, reduction in turbulent production terms. The growth rate of the later is related to the integrated turbulent production.[92] Therefore, a decrease in this production results in reduction of the layer growth rate. This is evidenced in Fig. 4 which shows the temporal evolution of the momentum thickness ($\delta_m$).[69] As Fig. 4 shows, the shear layer growth rate reduces with increasing the density ratio, and increasing the $Ma$ number. This is consistent with previous DNS results.[21,82,93] However, the spreading rates as predicted by the FDF are somewhat smaller than those by DNS. This was also observed in previous FDF simulations.[9]

Figures 5 to 8, 11 to 14 and 17 to 20 present several components of the resolved and SGS second-order moments. As observed, the PEVC-FMDF yields reasonable predictions. As a result, the total components also yield very good agreements with DNS data as shown in Figs. 9, 10, 15, 16, 21 and 22.

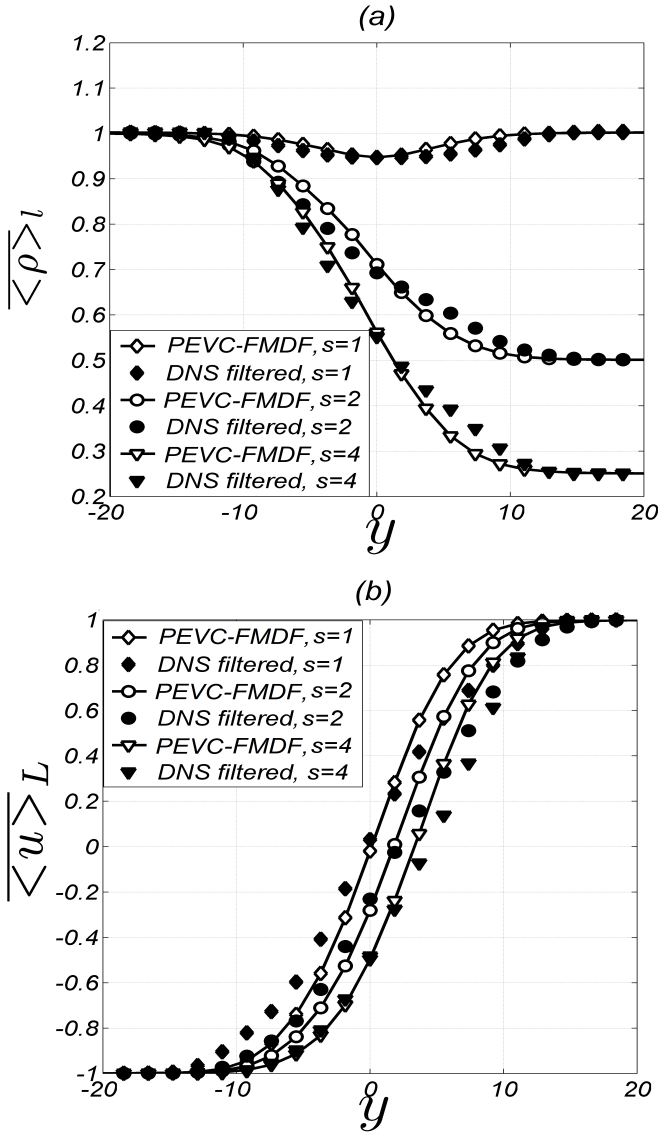


**Figure 3:** Cross-stream variation of Reynolds-averaged (a) $\overline{\langle \rho \rangle_\ell}$ and (b) $\overline{\langle u \rangle_L}$ with $Ma = 0.6$ at $t = 45$.

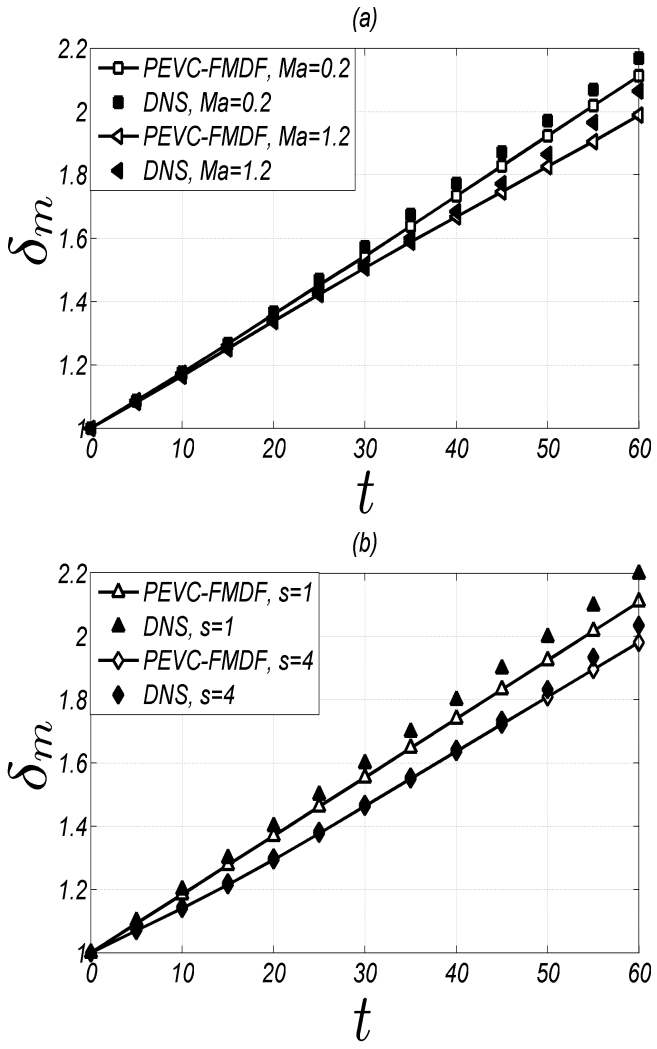


**Figure 4:** Temporal variation of the normalized momentum thickness: (a) $s = 2$, (b) $Ma = 1.2$.

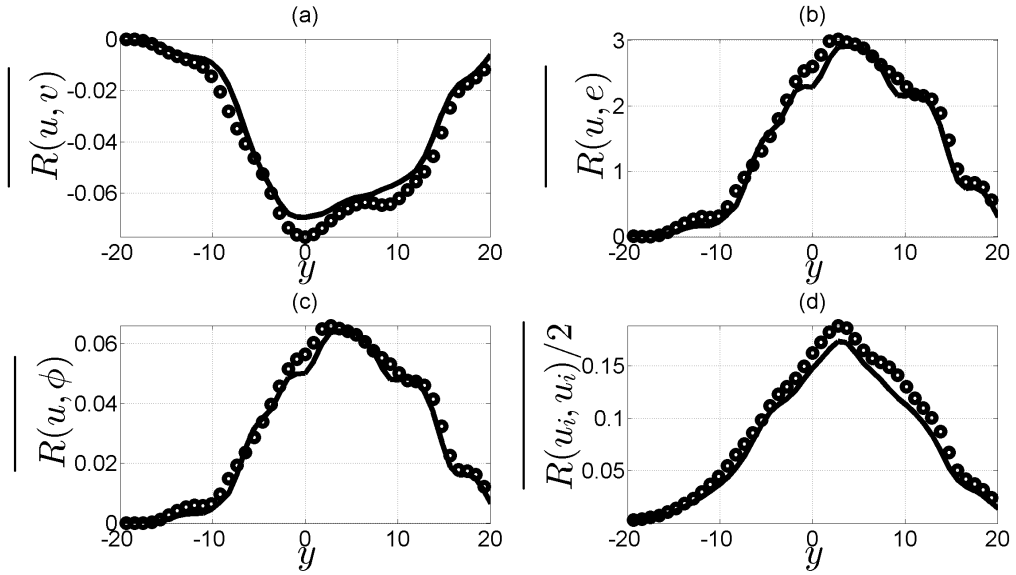


**Figure 5:** Cross-stream variation of some of the components of $\overline{R}$ at $t = 50$ with $Ma = 0.2$ and $s = 2$. The thick solid line denote LES predictions using PEVC-FMDF and circles show the DNS data.

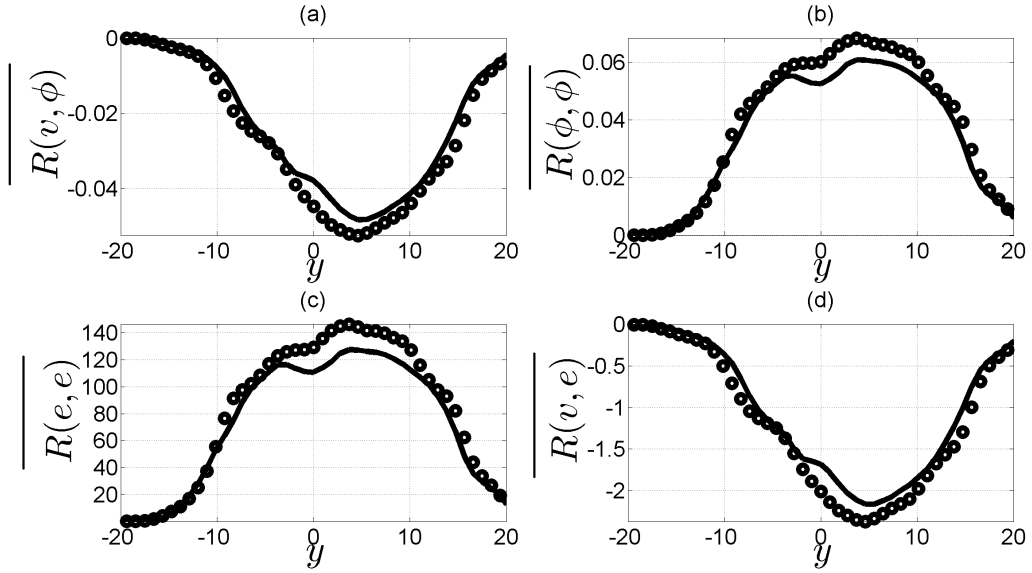


**Figure 6:** Cross-stream variation of some of the components of $\overline{R}$ at $t = 50$ with $Ma = 0.2$ and $s = 2$. The thick solid line denote LES predictions using PEVC-FMDF and circles show the DNS data.

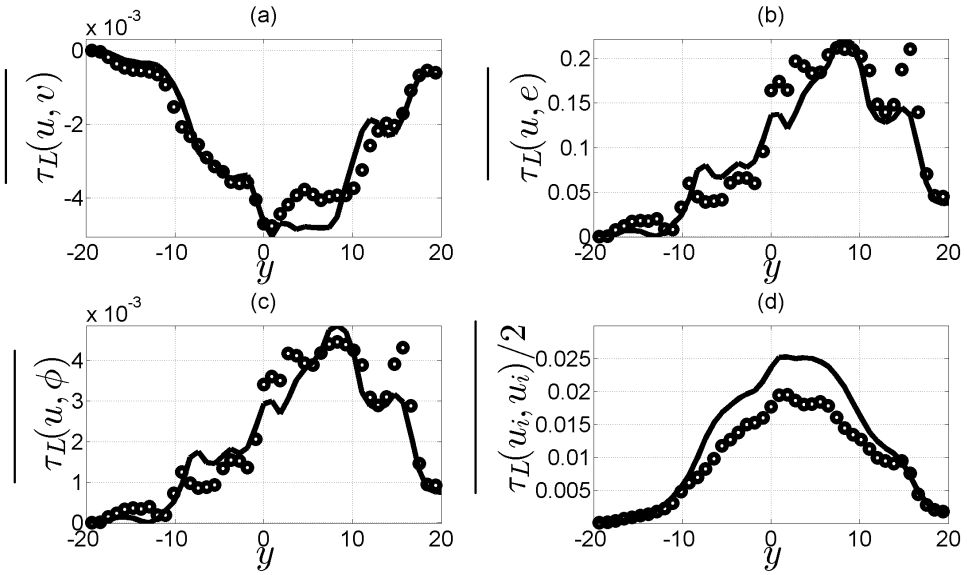


**Figure 7:** Cross-stream variation of some of the Reynolds-averaged components of $\overline{\tau_L}$ at $t = 50$ with $Ma = 0.2$ and $s = 2$. The thick solid line denote LES predictions using PEVC-FMDF and circles show the DNS data.

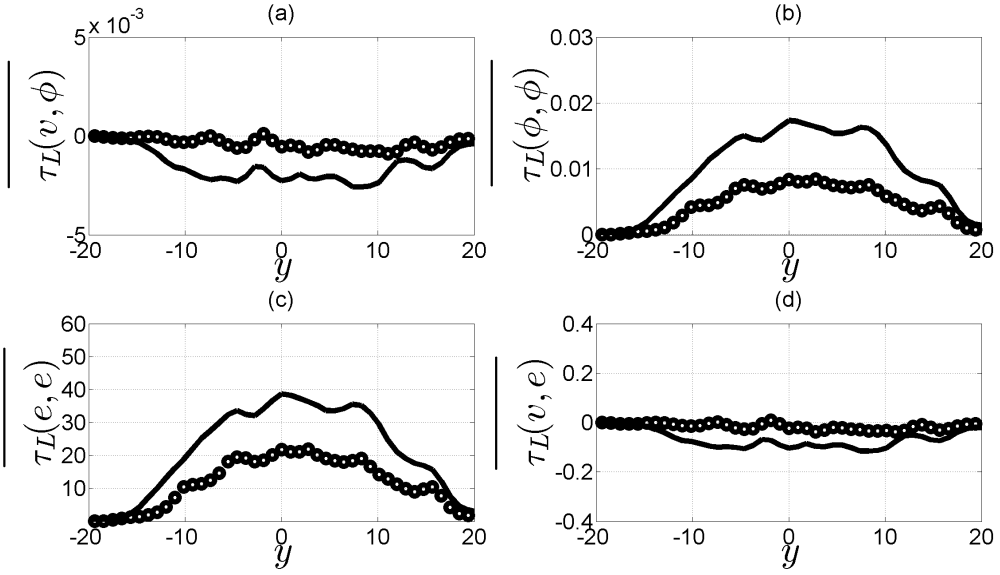


**Figure 8:** Cross-stream variation of some of the Reynolds-averaged components of $\overline{\tau_L}$ at $t = 50$ with $Ma = 0.2$ and $s = 2$. The thick solid line denote LES predictions using PEVC-FMDF and circles show the DNS data.

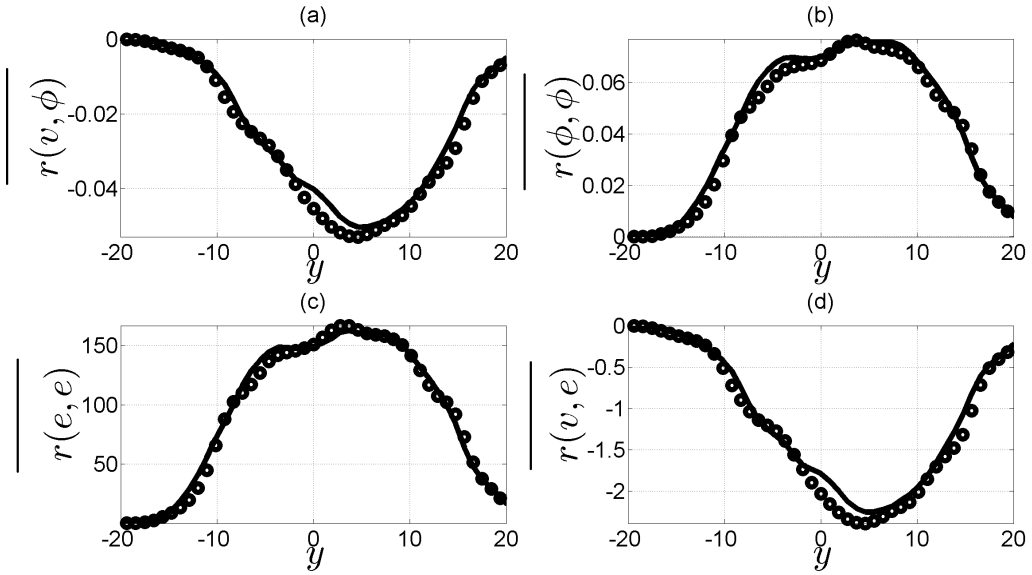


**Figure 9:** Cross-stream variation of some of the components of $\overline{r}$ at $t = 50$ with $Ma = 0.2$ and $s = 2$. The thick solid line denote LES predictions using PEVC-FMDF and circles show the DNS data.

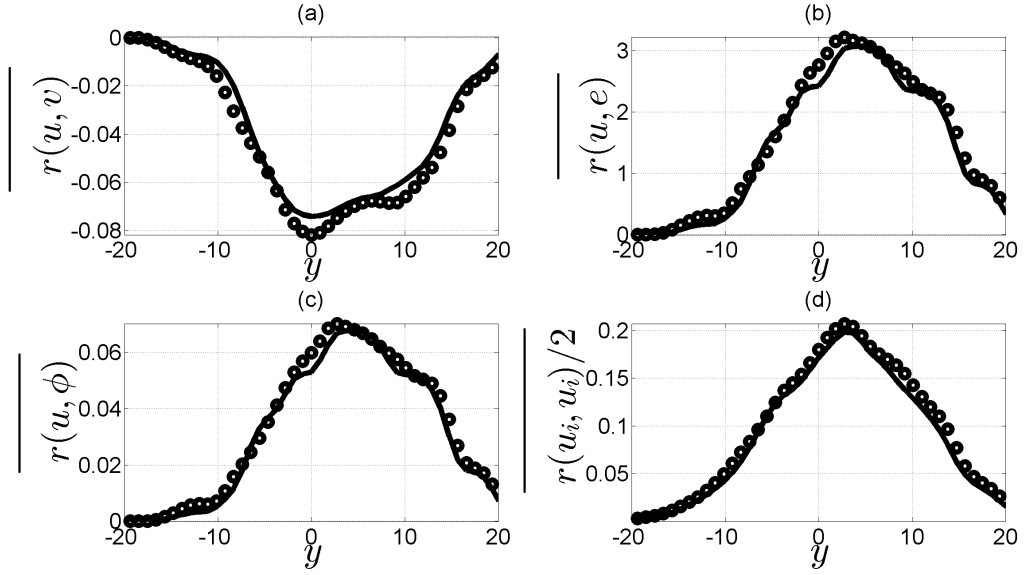


**Figure 10:** Cross-stream variation of some of the components of $\overline{r}$ at $t = 50$ with $Ma = 0.2$ and $s = 2$. The thick solid line denote LES predictions using PEVC-FMDF and circles show the DNS data.

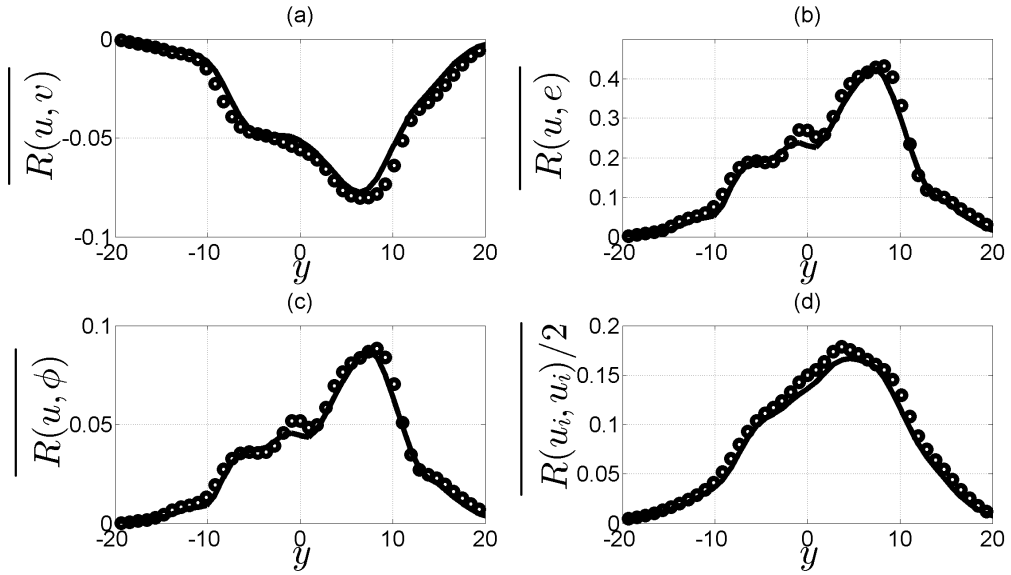


**Figure 11:** Cross-stream variation of some of the components of $\overline{R}$ at $t = 65$ with $Ma = 0.6$ and $s = 2$. The thick solid line denote LES predictions using PEVC-FMDF and circles show the DNS data.

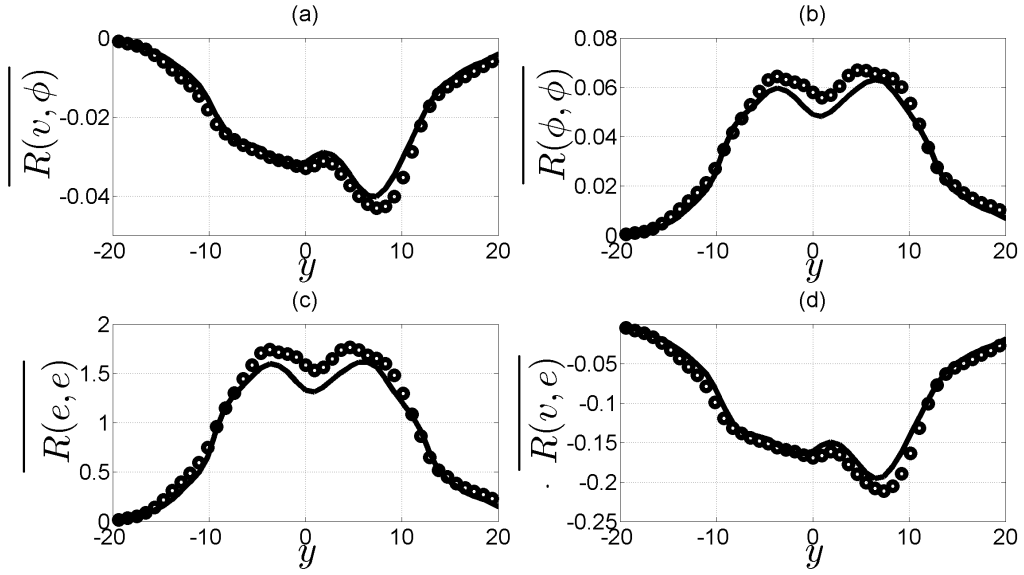


**Figure 12:** Cross-stream variation of some of the components of $\overline{R}$ at $t = 65$ with $Ma = 0.6$ and $s = 2$. The thick solid line denote LES predictions using PEVC-FMDF and circles show the DNS data.

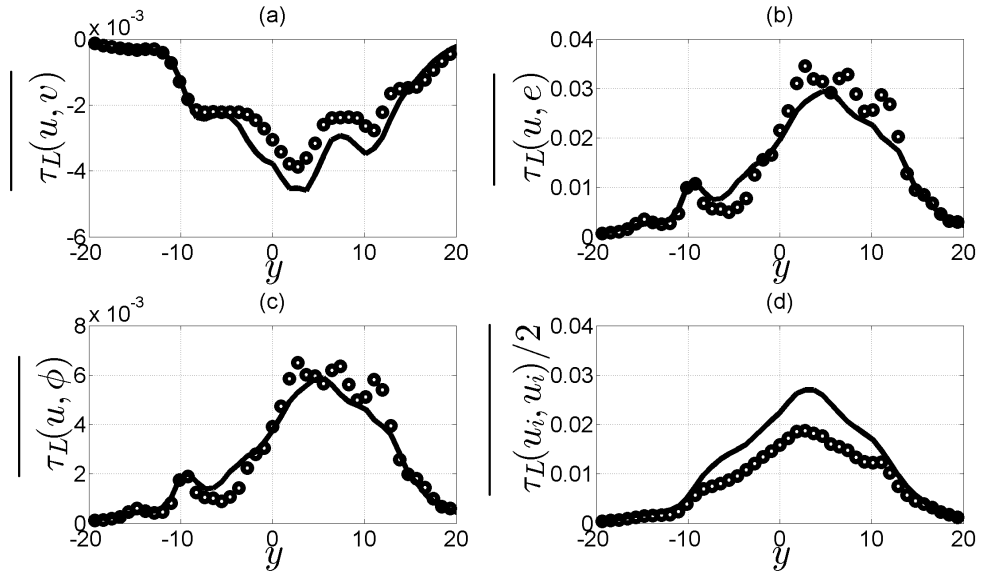


**Figure 13:** Cross-stream variation of some of the Reynolds-averaged components of $\overline{\tau_L}$ at $t = 65$ with $Ma = 0.6$ and $s = 2$. The thick solid line denote LES predictions using PEVC-FMDF and circles show the DNS data.

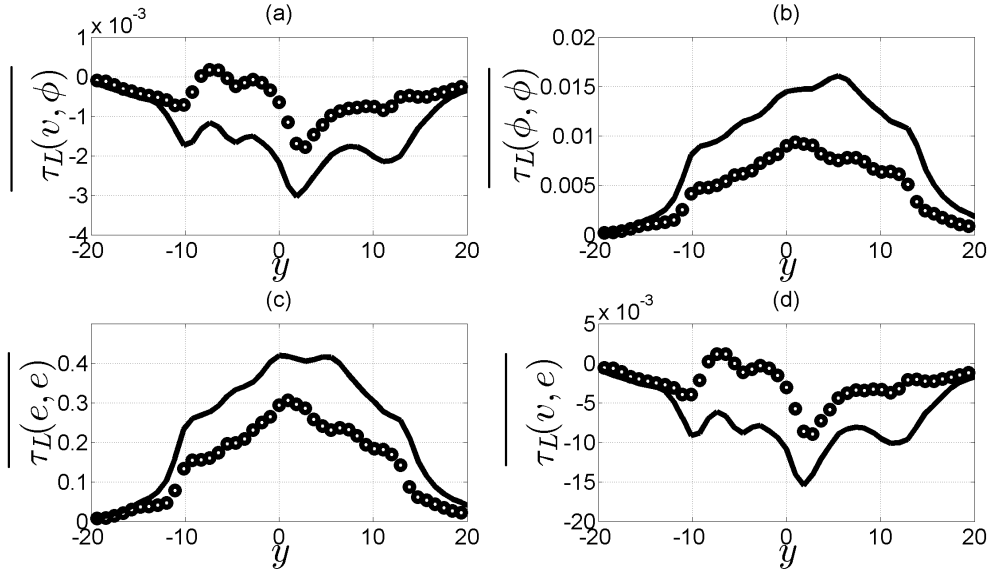


**Figure 14:** Cross-stream variation of some of the Reynolds-averaged components of $\overline{\tau_L}$ at $t = 65$ with $Ma = 0.6$ and $s = 2$. The thick solid line denote LES predictions using PEVC-FMDF and circles show the DNS data.

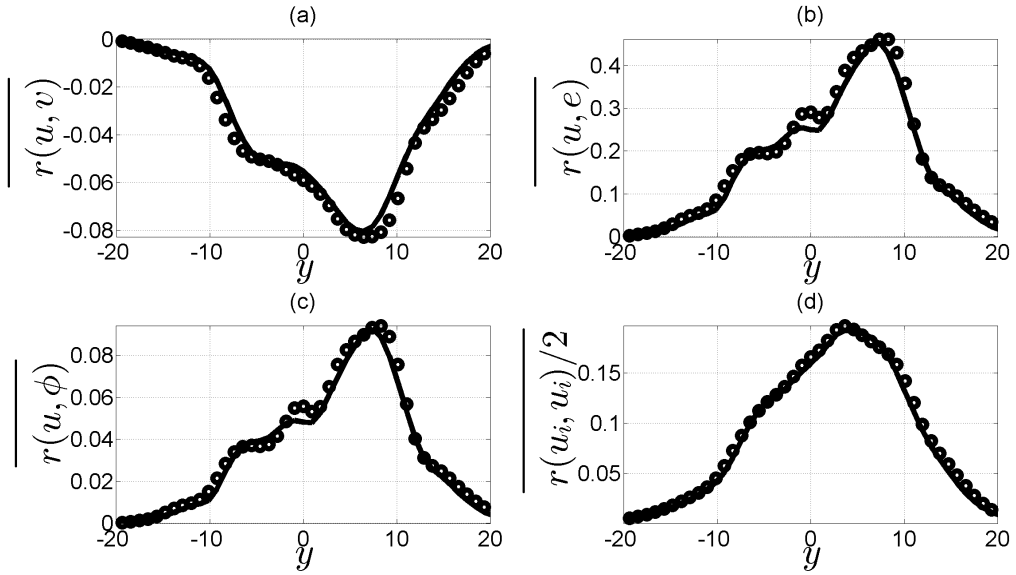


**Figure 15:** Cross-stream variation of some of the components of $\overline{r}$ at $t = 65$ with $Ma = 0.6$ and $s = 2$. The thick solid line denote LES predictions using PEVC-FMDF and circles show the DNS data.

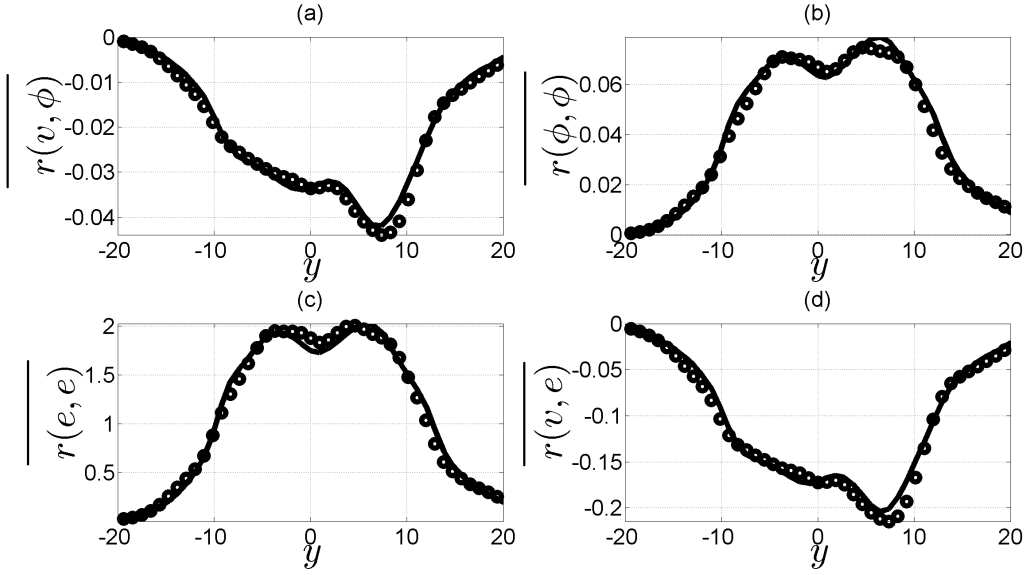


**Figure 16:** Cross-stream variation of some of the components of $\overline{r}$ at $t = 65$ with $Ma = 0.6$ and $s = 2$. The thick solid line denote LES predictions using PEVC-FMDF and circles show the DNS data.

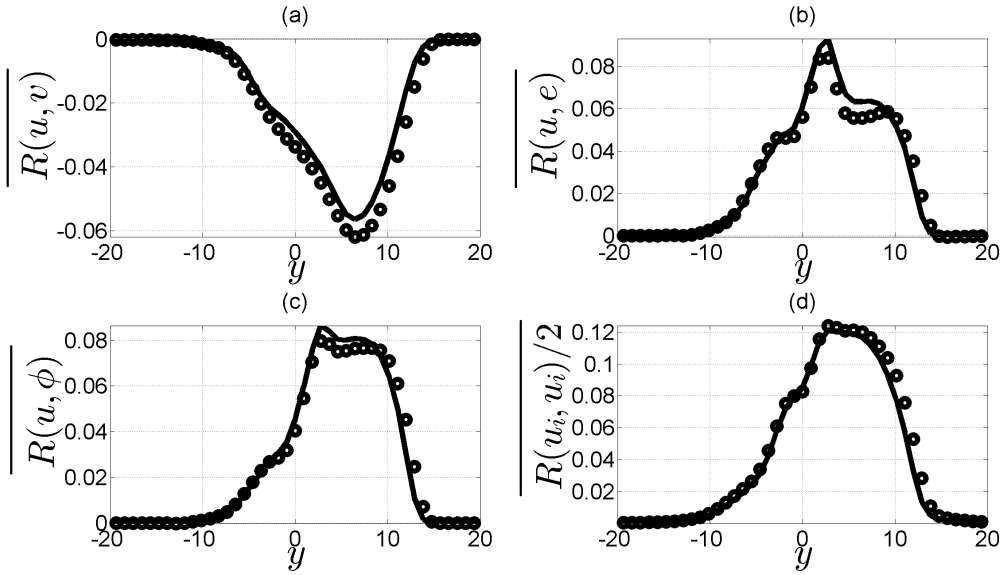


**Figure 17:** Cross-stream variation of some of the components of $\overline{R}$ at $t = 75$ with $Ma = 1.2$ and $s = 2$. The thick solid line denote LES predictions using PEVC-FMDF and circles show the DNS data.

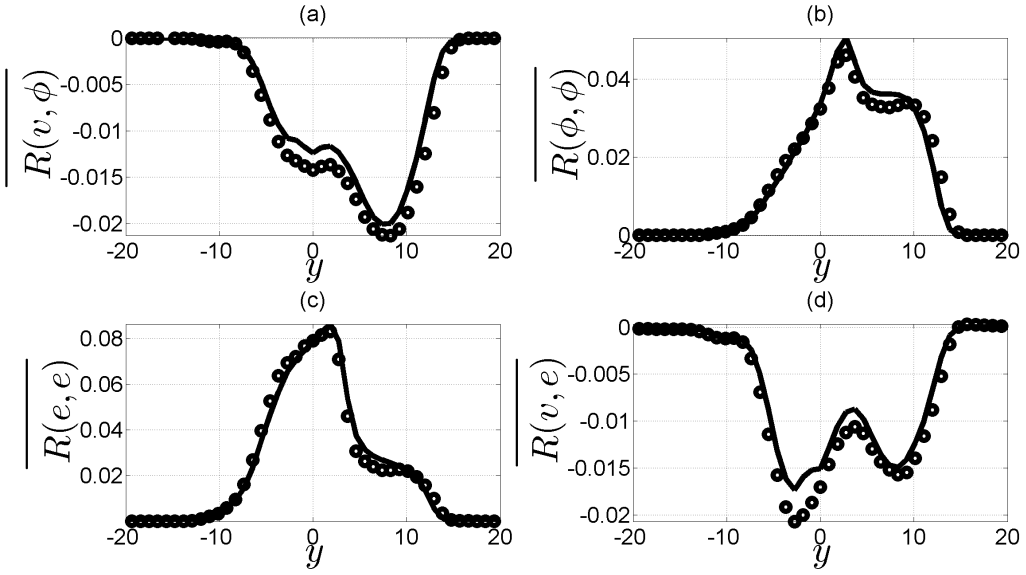


**Figure 18:** Cross-stream variation of some of the components of $\overline{R}$ at $t = 75$ with $Ma = 1.2$ and $s = 2$. The thick solid line denote LES predictions using PEVC-FMDF and circles show the DNS data.

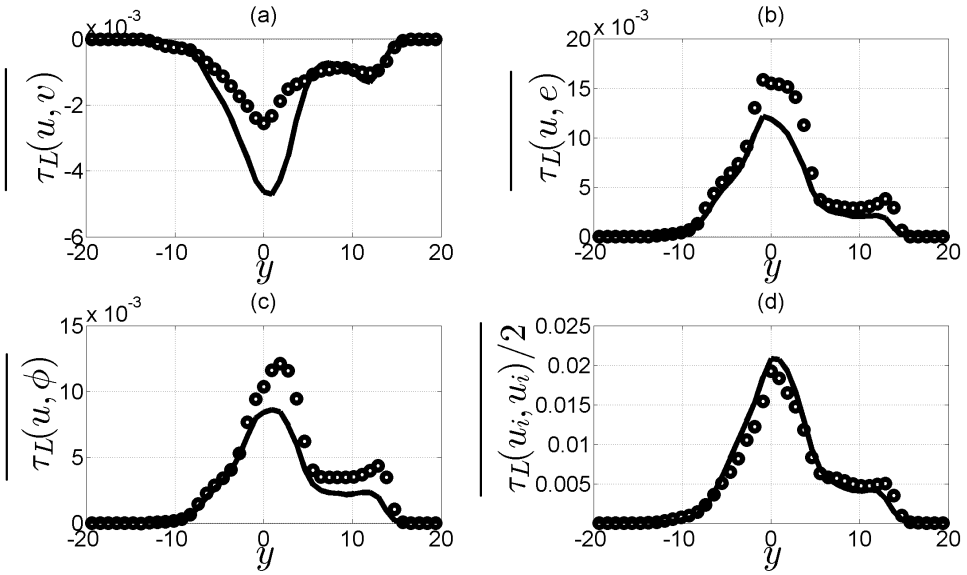


**Figure 19:** Cross-stream variation of some of the Reynolds-averaged components of $\overline{\tau_L}$ at $t = 75$ with $Ma = 1.2$ and $s = 2$. The thick solid line denote LES predictions using PEVC-FMDF and circles show the DNS data.

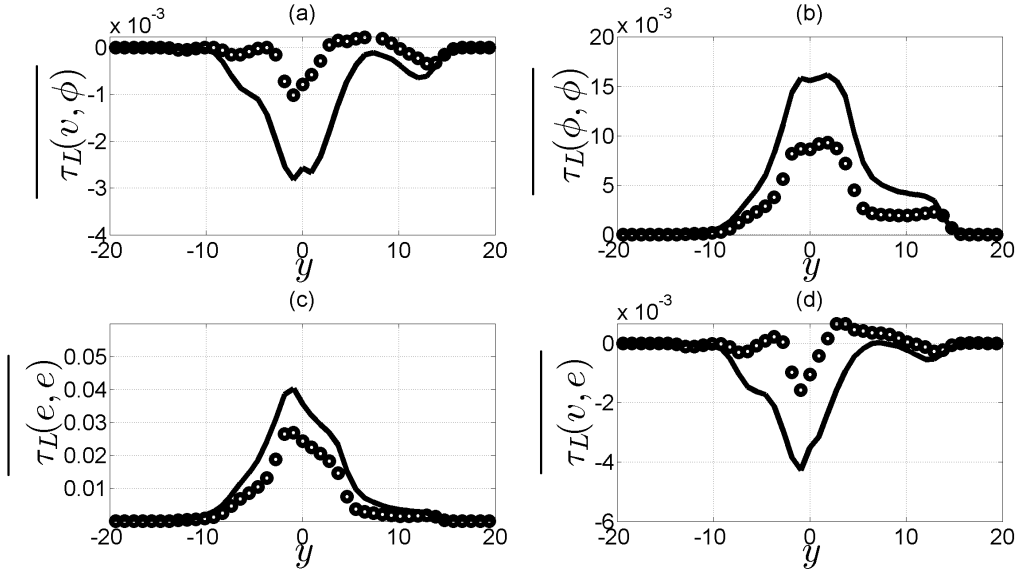


**Figure 20:** Cross-stream variation of some of the Reynolds-averaged components of $\overline{\tau_L}$ at $t = 75$ with $Ma = 1.2$ and $s = 2$. The thick solid line denote LES predictions using PEVC-FMDF and circles show the DNS data.

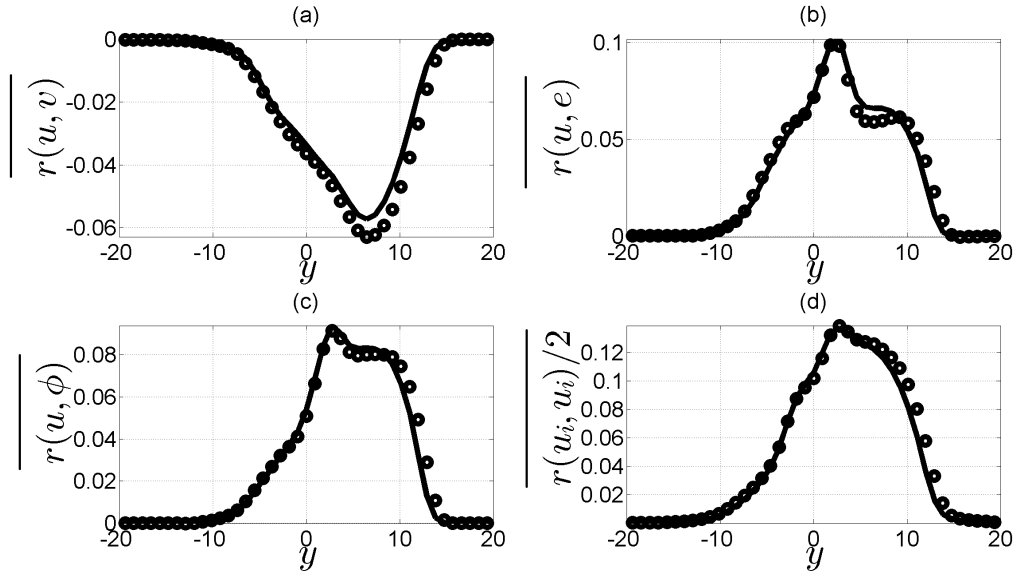


**Figure 21:** Cross-stream variation of some of the components of $\overline{r}$ at $t = 75$ with $Ma = 1.2$ and $s = 2$. The thick solid line denote LES predictions using PEVC-FMDF and circles show the DNS data.

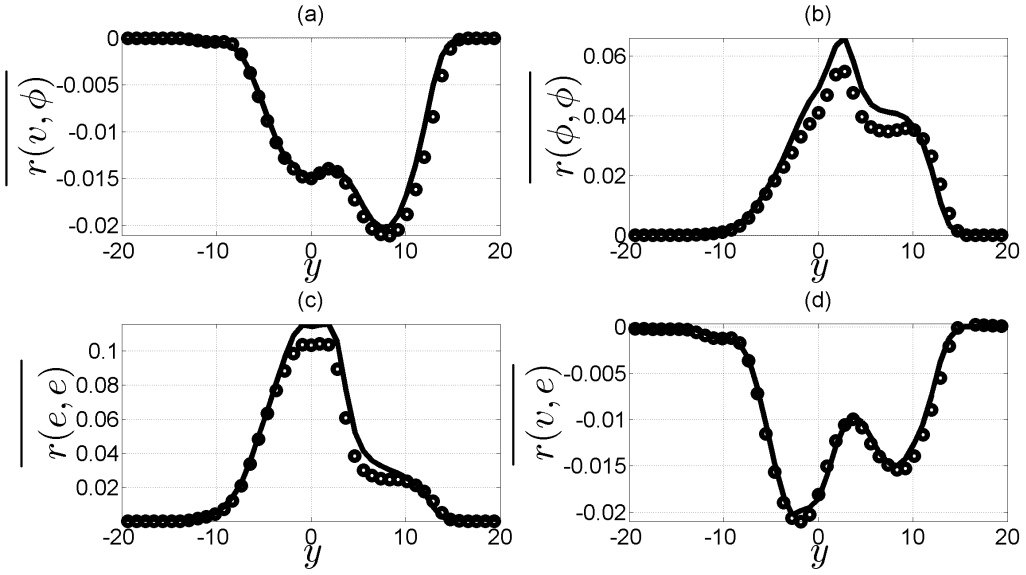


**Figure 22:** Cross-stream variation of some of the components of $\overline{r}$ at $t = 75$ with $Ma = 1.2$ and $s = 2$. The thick solid line denote LES predictions using PEVC-FMDF and circles show the DNS data.

## 5.0 SUMMARY & CONCLUSIONS

The filtered density function (FDF) has proven to be a very effective subgrid scale closure for large eddy simulation of turbulent reactive flows.[2,3] In all previous works, the FDF were considered for selected transport variables; the closure for other variables were provided by other means. The objective of the present work is to develop the FDF in a self-contained manner, accounting for SGS statistics of all of the transport variables. For this purpose, the pressure-energy-velocity-composition filtered mass density function (PEVC-FMDF) is developed. The exact transport equation governing the evolution of this FDF is derived. It is shown that the effect of SGS convection appears in a closed form. The unclosed terms are modeled in a fashion similar to that in probability density function methods. The capability of the PEVC-FMDF is demonstrated by conducting LES of a temporally developing mixing layer. The performance of the model as appraised by comparisons with DNS data is encouraging.

Future work must consider other kernels of the SLM coupled with more comprehensive SGS pressure-strain correlations, *e.g.* Refs.[94] Extension to LES of reactive flows is straightforward if reliable kinetics models are provided. Future applications to a broader class of flows with escalated degrees of complexity are also recommended. With these extension, LES of practical flows with this self-contained FDF becomes possible, as is currently the case with scalar-FDF.[40]

## BIBLIOGRAPHY


[1] Miller, R. S. and Foster, J. W., Survey of Turbulent Combustion Models for Large-Eddy Simulations of Propulsive Flowfields, *AIAA J.*, **54**(10):2930–2946 (2016).

[2] Pope, S. B., Small Scales, Many Species and the Manifold Challenges of Turbulent Combustion, *Proc. Combust. Inst.*, **34**(1):1–31 (2013).

[3] Haworth, D. C., Progress in Probability Density Function Methods for Turbulent Reacting Flows, *Prog. Energ. Combust.*, **36**(2):168–259 (2010).

[4] Yilmaz, S. L., Ansari, N., Pisciuneri, P. H., Nik, M. B., Otis, C. C., and Givi, P., Applied Filtered Density Function, *J. Appl. Fluid Mech.*, **6**(3):311–320 (2013).

[5] Kuo, K. K. and Acharya, R., *Fundamentals of Turbulent and Multiphase Combustion*, John Wiley & Sons Inc., Hoboken, NJ, 2012.

[6] Ansari, N., Jaberi, F. A., Sheikhi, M. R. H., and Givi, P., Filtered Density Function as a Modern CFD Tool, in Maher, A. R. S., editor, *Engineering Applications of Computational Fluid Dynamics: Volume 1*, Chapter 1, pp. 1–22, International Energy and Environment Foundation, 2011.

[7] Almeida, T., Afshari, A., and Jaberi, F. A., Modeling and Large-Scale Simulations of Complex Combustion Systems, in Roy, G. D., Yu, K. H., Whitelaw, J. H., and Witton, J. J., editors, *Advances in Combustion and Noise Control*, Chapter 35, pp. 551–564, Cranfield University Press, Cranfield, England, 2006.

[8] Givi, P., Filtered Density Function for Subgrid Scale Modeling of Turbulent Combustion, *AIAA J.*, **44**(1):16–23 (2006).

[9] Sheikhi, M. R. H., Givi, P., and Pope, S. B., Frequency-Velocity-Scalar Filtered Mass Density Function for Large Eddy Simulation of Turbulent Flows, *Phys. Fluids*, **21**(7):075102 (2009).

[10] Nik, M. B., Yilmaz, S. L., Givi, P., Sheikhi, M. R. H., and Pope, S. B., Simulation of Sandia Flame D using Velocity-Scalar Filtered Density Function, *AIAA J.*, **48**(7):1513–1522 (2010).

[11] Sheikhi, M. R. H., Givi, P., and Pope, S. B., Velocity-Scalar Filtered Mass Density Function for Large Eddy Simulation of Turbulent Reacting Flows, *Phys. Fluids*, **19**(9):095106 (2007).

[12] Sheikhi, M. R. H., Drozda, T. G., Givi, P., and Pope, S. B., Velocity-Scalar Filtered Density Function for Large Eddy Simulation of Turbulent Flows, *Phys. Fluids*, **15**(8):2321–2337 (2003).

[13] Safari, M. and Sheikhi, M. R. H., Large Eddy Simulation-Based Analysis of Entropy Generation in a Turbulent Nonpremixed Flame, *Energy*, **78**:451–457 (2014).

[14] Safari, M., Hadi, F., and Sheikhi, M. R. H., Progress in the Prediction of Entropy Generation in Turbulent Reacting Flows using Large Eddy Simulation, *Entropy*, **16**(10):5159–5177 (2014).

[15] Sheikhi, M. R. H., Safari, M., and Hadi, F., Entropy Filtered Density Function for Large Eddy Simulation of Turbulent Flows, *AIAA J.*, **53**(9):2571–2587 (2015).

[16] Li, Z., Banaeizadeh, A., and Jaberi, F. A., Two-Phase Filtered Mass Density Function for LES of Turbulent Reacting Flows, *J. Fluid Mech.*, **760**:243–277 (2014).

[17] Irannejad, A. and Jaberi, F. A., Large Eddy Simulation of Turbulent Spray Combustion, *Combust. Flame*, **162**:431–450 (2015).

[18] Gicquel, L. Y. M., Givi, P., Jaberi, F. A., and Pope, S. B., Velocity Filtered Density Function for Large Eddy Simulation of Turbulent Flows, *Phys. Fluids*, **14**(3):1196–1213 (2002).

[19] Colucci, P. J., Jaberi, F. A., Givi, P., and Pope, S. B., Filtered Density Function for Large Eddy Simulation of Turbulent Reacting Flows, *Phys. Fluids*, **10**(2):499–515 (1998).

[20] Pope, S. B., Computations of Turbulent Combustion: Progress and Challenges, *Proc. Combust. Inst.*, **23**(1):591–612 (1990).

[21] Givi, P., Model-Free Simulations of Turbulent Reactive Flows, *Prog. Energ. Combust.*, **15**(1):1–107 (1989).

[22] Gao, F. and O'Brien, E. E., A Large-Eddy Simulation Scheme for Turbulent Reacting Flows, *Phys. Fluids A*, **5**(6):1282–1284 (1993).

[23] Colucci, P. J., Jaberi, F. A., Givi, P., and Pope, S. B., Filtered Density Function for Large Eddy Simulation of Turbulent Reacting Flows, *Phys. Fluids*, **10**(2):499–515 (1998).

[24] Jaberi, F. A., Colucci, P. J., James, S., Givi, P., and Pope, S. B., Filtered Mass Density Function for Large-Eddy Simulation of Turbulent Reacting Flows, *J. Fluid Mech.*, **401**:85–121 (1999).

[25] Yilmaz, S. L., Nik, M. B., Givi, P., and Strakey, P. A., Scalar Filtered Density Function for Large Eddy Simulation of a Bunsen Burner, *J. Propul. Power*, **26**(1):84–93 (2010).

[26] Nik, M. B., Yilmaz, S. L., Sheikhi, M. R. H., and Givi, P., Grid Resolution Effects on VSFMDF/LES, *Flow Turbul. Combust.*, **85**(3–4):677–688 (2010).

[27] Yilmaz, S. L., Nik, M. B., Sheikhi, M. R. H., Strakey, P. A., and Givi, P., An Irregularly Portioned Lagrangian Monte Carlo Method for Turbulent Flow Simulation, *J. Sci. Comput.*, **47**(1):109–125 (2011).

[28] Ansari, N., Pisciuneri, P. H., Strakey, P. A., and Givi, P., Scalar-Filtered Mass-Density-Function Simulation of Swirling Reacting Flows on Unstructured Grids, *AIAA J.*, **50**(11):2476–2482 (2012).

[29] Rowinski, D. H. and Pope, S. B., Computational Study of Lean Premixed Turbulent Flames using RANSPDF and LESPDF Methods, *Combus. Theor. Model.*, **17**(4):610–656 (2013).

[30] Sawford, B. L., Pope, S. B., and Yeung, P. K., Gaussian Lagrangian Stochastic Models for Multi-Particle Dispersion, *Phys. Fluids*, **25**(5):055101 (2013).

[31] Banaeizadeh, A., Afshari, A., Schock, H., and Jaberi, F. A., Large Eddy Simulations of Turbulent Flows in Internal Combustion Engines, *Int. J. Heat Mass Tran.*, **60**:781–796 (2013).

[32] Pisciuneri, P. H., Yilmaz, S. L., Strakey, P. A., and Givi, P., An Irregularly Portioned FDF Simulator, *SIAM J. Sci. Comput.*, **35**(4):C438–C452 (2013).

[33] Yang, Y., Wang, H., Pope, S. B., and Chen, J. H., Large-Eddy Simulation/Probability Density Function Modeling of a Non-Premixed CO/H2 Temporally Evolving Jet Flame, *Proc. Combust. Inst.*, **34**(1):1241–1249 (2013).

[34] Kim, J. and Pope, S. B., Effects of Combined Dimension Reduction and Tabulation on the Simulations of a Turbulent Premixed Flame using a Large-Eddy Simulation/Probability Density Function Method, *Combust. Theo. Model.*, **18**(3):388–413 (2014).

[35] Minier, J., Chibbaro, S., and Pope, S. B., Guidelines for the Formulation of Lagrangian Stochastic Models for Particle Simulations of Single-Phase and Dispersed Two-Phase Turbulent Flows, *Phys. Fluids*, **26**(11):113303 (2014).

[36] Popov, P. P. and Pope, S. B., Large Eddy Simulation/Probability Density Function Simulations of Bluff Body Stabilized Flames, *Combust. Flame*, **161**(12):3100–3133 (2014).

[37] Dodoulas, I. A. and Navarro-Martinez, S., Analysis of Extinction in a Non-Premixed Turbulent Flame using Large Eddy Simulation and the Chemical Explosion Mode Analysis, *Combust. Theo. Model.*, **19**(1):107–129 (2015).

[38] Jones, W. P., Marquis, A. J., and Noh, D., LES of a Methanol Spray Flame with a Stochastic Sub-Grid Model, *Proc. Combust. Inst.*, **35**(2):1685–1691 (2015).

[39] Pisciuneri, P. H., Yilmaz, S. L., Strakey, P. A., and Givi, P., Massively Parallel FDF Simulation of Turbulent Reacting Flows, in Heinz, S. and Bessaih, H., editors, *Stochastic Equations for Complex Systems: Theoretical and Computational Topics*, Mathematical Engineering, Chapter 8, pp. 175–192, Springer, 2015.

[40] Ansari, N., Strakey, P. A., Goldin, G., and Givi, P., Filtered Density Function Simulation of a Realistic Swirled Combustor, *Proc. Combust. Inst.*, **35**(2):1433–1442 (2015).

[41] Esmaelli, M., Afshari, A., and Jaberi, F. A., Turbulent Mixing in Non-Isothermal Jet in Cross-Flow, *Int. J. Heat Mass Tran.*, **89**:1239–1257 (2015).

[42] Liang, Y., Pope, S. B., and Pepiot, P., A Pre-Partitioned Adaptive Chemistry Methodology for the Efficient Implementation of Combustion Chemistry in Particle PDF Methods, *Combust. Flame*, **162**(9):3236–3253 (2015).

[43] Sammak, S., Brazell, M. J., Givi, P., and Mavriplis, D. J., A Hybrid DG-Monte Carlo FDF Simulator, *Comput. Fluids*, **140**(13):158–166 (2016).

[44] Tirunagari, R. R. and Pope, S. B., LES/PDF for Premixed Combustion in the DNS Limit, *Combust. Theo. Model.*, **20**(5):1–32 (2016).

[45] Tirunagari, R. R. and Pope, S. B., An Investigation of Turbulent Premixed Counterflow Flames using Large-Eddy Simulations and Probability Density Function Methods, *Combust. Flame*, **166**:229–242 (2016).

[46] Jones, W. P., Marquis, A. J., and Noh, D., A Stochastic Breakup Model for Large Eddy Simulation of a Turbulent Two-Phase Reactive Flow, *Proc. Combust. Inst.*, **36**(2):2559–2566 (2017).

[47] Sammak, S., Nouri, A. G., Brazell, M. J., Mavriplis, D. J., and Givi, P., Discontinuous Galerkin-Monte Carlo Solver for Large Eddy Simulation of Compressible Turbulent Flows, in *55th AIAA Aerospace Sciences Meeting*, pp. 1–13, Grapevine, TX, 2017, AIAA-2017-0982.

[48] Banaeizadeh, A., Li, Z., and Jaberi, F. A., Compressible Scalar Filtered Density Function Model for High-Speed Turbulent Flows, *AIAA J.*, **49**(10):2130–2143 (2011).

[49] Nik, M. B., Givi, P., Madnia, C. K., and Pope, S. B., EPVS-FMDF for LES of High-Speed Turbulent Flows, in *50th AIAA Aerospace Sciences Meeting Including the New Horizons Forum and Aerospace Exposition*, Nashville, TN, 2012, AIAA-2012-0117.

[50] Drozda, T. G., Quinlan, J. R., Pisciuneri, P. H., and Yilmaz, S. L., Progress Toward Affordable High Fidelity Combustion Simulations for High-Speed Flows in Complex Geometries, in *48th AIAA/ASME/SAE/ASEE Joint Propulsion Conference and Exhibit*

*and 10th International Energy Conversion Engineering Conference*, Atlanta, GA, 2012, AIAA-2012-4264.

[51] Nouri, A. G., Givi, P., Nik, M. B., and Pope, S. B., Pressure-Velocity Filtered Mass Density Function for Large Eddy Simulation of Compressible Turbulent Flow, in *International Conference on Model Integration across Disparate Scales in Complex Turbulent Flow Simulation*, State College, PA, 2015.

[52] Nouri, A. G., Givi, P., Nik, M. B., and Pope, S. B., Pressure-Velocity-Scalar Filtered Mass Density Function for Large Eddy Simulation of Compressible Turbulent Flow, in *Bulletin of the American Physical Society, 68th Annual Meeting of the APS Division of Fluid Dynamics*, Vol. 60, p. 565, Boston, MA, 2015, American Physical Society.

[53] Nouri, A. G., Givi, P., and Layton, W., Modeling and Simulation of Turbulence not at Statistical Equilibrium, in *Bulletin of the American Physical Society, 69th Annual Meeting of the APS Division of Fluid Dynamics*, Vol. 61, p. 271, Portland, OR, 2016, American Physical Society.

[54] Nouri, A. G., Nik, M. B., Givi, P., Livescu, D., and Pope, S. B., PEVC-FMDF for Large Eddy Simulation of Compressible Turbulent Flows, in *Bulletin of the American Physical Society, 70th Annual Meeting of the APS Division of Fluid Dynamics*, In Press, Denver, CO, 2017, American Physical Society.

[55] Nouri, A. G., Nik, M. B., Givi, P., Livescu, D., and Pope, S. B., Self-Contained Filtered Density Function, *Phys. Rev. Fluids*, **2**:094603 (2017).

[56] Sammak, S., Nouri, A. G., Ansari, N., and Givi, P., Quantum Computing and Its Potential for Turbulence Simulations, in Danaev, N., Shokin, Y., and Akhmed-Zakin, D., editors, *Mathematical Modeling of Technological Processes*, Communications in Computer and Information Science, Chapter 13, pp. 124–132, Springer, 2015.

[57] Nouri, A. G., Sammak, S., Pisciuneri, P. H., and Givi, P., Langevin Simulation of Turbulent Combustion, in Agarwal, A. K., De, S., Pandy, A., and Singh, A. P, editors, *Combustion for Power Generation and Transportation: Technology, Challenges and Prospects*, pp. 39–53, Springer, Singapore, 2017.

[58] Libby, P. A. and Williams, F. A., *Turbulent Reacting Flows*, *Topics in Applied Physics*, Vol. 44, Springer-Verlag, Heidelberg, 1980.

[59] Pope, S. B., PDF Methods for Turbulent Reactive Flows, *Prog. Energ. Combust.*, **11**(2):119–192 (1985).

[60] Bilger, R. W., Molecular Transport Effects in Turbulent Diffusion Flames at Moderate Reynolds Number, *AIAA J.*, **20**:962–970 (1982).

[61] Poinsot, T. and Veynante, D., *Theoretical and Numerical Combustion*, R. T. Edwards, Inc., Bordeaux, France, third edition, 2012.

[62] Pope, S. B., *Turbulent Flows*, Cambridge University Press, Cambridge, U.K., 2000.

[63] Piomelli, U., Large-Eddy Simulation: Achievements and Challenges, *Prog. Aerosp. Sci.*, **35**(4):335–362 (1999).

[64] Meneveau, C. and Katz, J., Scale-Invariance and Turbulence Models for Large-Eddy Simulation, *Annu. Rev. Fluid Mech.*, **32**:1–32 (2000).

[65] Geurts, B. J., *Modern Simulation Strategies for Turbulent Flow*, R. T. Edwards, Inc., Philadelphia, PA, 2001.

[66] Sagaut, P., *Large Eddy Simulation for Incompressible Flows*, Springer-Verlag, New York, NY, third edition, 2005.

[67] Germano, M., Turbulence: the Filtering Approach, *J. Fluid Mech.*, **238**:325–336 (1992).

[68] O'Brien, E. E., The Probability Density Function (PDF) Approach to Reacting Turbulent Flows, in Libby, P. and Williams, F., editors, *Turbulent Reacting Flows*, *Topics in Applied Physics*, Vol. 44, Chapter 5, pp. 185–218, Springer, Heidelberg, 1980.

[69] Vreman, B., Geurts, B., and Kuerten, H., Realizability Conditions for the Turbulent Stress Tensor in Large-Eddy Simulation, *J. Fluid Mech.*, **278**:351–362 (1994).

[70] Wax, N., *Selected Papers on Noise and Stochastic Processes*, Dover, 1954.

[71] Delarue, B. J. and Pope, S. B., Application of PDF Methods to Compressible Turbulent Flows, *Phys. Fluids*, **9**(9):2704–2715 (1997).

[72] Delarue, B. J. and Pope, S. B., Calculations of Subsonic and Supersonic Turbulent Reacting Mixing Layers using Probability Density Function Methods, *Phys. Fluids*, **10**(2):487–498 (1998).

[73] Haworth, D. C. and Pope, S. B., A Generalized Langevin Model for Turbulent Flows, *Phys. Fluids*, **29**(2):387–405 (1986).

[74] Dreeben, T. D. and Pope, S. B., Probability Density Function and Reynolds-Stress Modeling of Near-Wall Turbulent Flows, *Phys. Fluids*, **9**(1):154–163 (1997).

[75] Dopazo, C. and O'Brien, E. E., Statistical Treatment of Non-Isothermal Chemical Reactions in Turbulence, *Combust. Sci. Technol.*, **13**(1–6):99–122 (1976).

[76] Martin, M. P., Piomelli, U., and Candler, G. V., Subgrid-Scale Models for Compressible Large-Eddy Simulations, *Theor. Comp. Fluid Dyn.*, **13**(5):361–376 (2000).

[77] Risken, H., *The Fokker-Planck Equation, Methods of Solution and Applications*, Springer-Verlag, New York, NY, 1989.

[78] Muradoglu, M., Pope, S. B, and Caughey, D. A., The Hybrid Method for the PDF Equations of Turbulent Reactive Flows: Consistency Conditions and Correction Algorithms, *J. Comput. Phys.*, **172**(2):841–878 (2001).

[79] Kloeden, P. E., Platen, E., and Schurz, H., *Numerical Solution of Stochastic Differential Equations through Computer Experiments*, Springer, Berlin; New York, second edition, 1997.

[80] Gikhman, I. I. and Skorokhod, A. V., *Stochastic Differential Equations*, Springer-Verlag, New York, NY, 1972.

[81] Muradoglu, M., Jenny, P., Pope, S. B., and Caughey, D. A., A Consistent Hybrid Finite-Volume/Particle Method for the PDF Equations of Turbulent Reactive Flows, *J. Comput. Phys.*, **154**(2):342–371 (1999).

[82] McMurtry, P. A., Jou, W.-H., Riley, J. J., and Metcalfe, R. W., Direct Numerical Simulations of a Reacting Mixing Layer with Chemical Heat Release, *AIAA J.*, **24**:962–970 (1986).

[83] Moser, R. D. and Rogers, M. M., The Three-Dimensional Evolution of a Plane Mixing Layer: Pairing and Transition to Turbulence, *J. Fluid Mech.*, **247**:275–320 (1993).

[84] Vreman, B., Geurts, B., and Kuerten, H., Large-Eddy Simulation of the Turbulent Mixing Layer, *J. Fluid Mech.*, **339**:357–390 (1997).

[85] Poinsot, T. J. and Lele, S. K., Boundary Conditions for Direct Simulations of Compressible Viscous Flows, *J. Comput. Phys.*, **101**(1):104–129 (1992).

[86] Erlebacher, G., Hussaini, M. Y., Speziale, C. G., and Zang, T. A., Toward the Large-Eddy Simulation of Compressible Turbulent Flows, *J. Fluid Mech.*, **238**:155–185 (1992).

[87] Pope, S. B., Ten Questions Concerning the Large-Eddy Simulation of Turbulent Flows, *New J. Phys.*, **6**(1):35 (2004).

[88] Giridhar, J., A Framework for Large Eddy Simulation of Incompressible Flows with Error Control, Ph.D. Thesis, Sibley School of Mechanical and Aerospace Engineering, Cornell University, Ithaca, NY, 2005.

[89] Pope, S. B., On the Relation Between Stochastic Lagrangian Models of Turbulence and Second-Moment Closures, *Phys. Fluids*, **6**(2):973–985 (1994).

[90] Metcalfe, R. W., Orszag, S. A., Brachet, M. E., Menon, S., and Riley, J. J., Secondary Instabilities of a Temporally Growing Mixing Layer, *J. Fluid Mech.*, **184**:207–243 (1987).

[91] Pantano, C. and Sarkar, S., A Study of Compressibility Effects in the High-Speed Turbulent Shear Layer using Direct Simulation, *J. Fluid Mech.*, **451**:329–371 (2002).

[92] Vreman, A. W., Sandham, N. D., and Luo, K. H., Compressible Mixing Layer Growth Rate and Turbulence Characteristics, *J. Fluid Mech.*, **320**:235–258 (1996).

[93] Givi, P., Madnia, C. K., Steinberger, C. J., Carpenter, M. H., and Drummond, J. P., Effects of Compressibility and Heat Release in a High Speed Reacting Mixing Layer, *Combust. Sci. Technol.*, **78**:33–68 (1991).

[94] Mishra, A. A. and Girimaji, S. S., On The Realizability Of Pressure-Strain Closures, *J. Fluid Mech.*, **755**:535–560 (2014).